1. Report No.	2. Government Accession No.	3. Recipient's Catalog No.
FHWA/TX-02/0-1708-2		

4. Title and Subtitle	5. Report Date
PREDICTING HOT-MIX PERFORMANCE FROM MEASURED PROPERTIES: PHASE II PROJECT DOCUMENTATION	November 2001
	6. Performing Organization Code
7. Author(s)	8. Performing Organization Report No.
Emmanuel Fernando, Tom Scullion, and Soheil Nazarian	Report 0-1708-2
9. Performing Organization Name and Address	10. Work Unit No. (TRAIS)
Texas Transportation Institute The Texas A&M University System College Station, Texas 77843-3135	11. Contract or Grant No. Project No. 0-1708
12. Sponsoring Agency Name and Address	13. Type of Report and Period Covered
Texas Department of Transportation Research and Technology Implementation Office P. O. Box 5080 Austin, Texas 78763-5080	Technical Report: September 2000 - August 2001
	14. Sponsoring Agency Code

15. Supplementary Notes

Research performed in cooperation with the Texas Department of Transportation and the U.S. Department of Transportation, Federal Highway Administration.
Research Project Title: Predicting Hot-Mix Performance from Measured Properties

16. Abstract

The problem of providing pavements that perform as designed is a major concern among state transportation agencies. Of importance in addressing this problem is the recognition that performance should drive not only the design process but also the construction process. This approach would necessitate the development of materials and construction specifications that are tied to pavement performance and the development of test equipment and procedures to evaluate the quality of the contractor's work based on predicted performance. In this way, engineers may test and accept as-built pavements on the basis of properties that are used in pavement design and are known to be determinants of pavement life.

Project 0-1708, "Predicting Hot-Mix Performance from Measured Properties," was initiated by the Texas Department of Transportation (TxDOT) to develop simple, practical, and reliable test procedures for evaluating the quality of hot-mix asphalt concrete pavements on the basis of predicted performance. To accomplish this objective, TxDOT established a three-phased work plan that called for: 1) conducting a detailed review of recent and ongoing related studies at the state and federal level (Phase I); 2) identifying mixture-, construction-, and structural-related properties that are significant predictors of pavement performance and are under the contractor's control (Phase II); and 3) identifying/modifying existing procedures or developing new procedures that relate the properties identified in Phase II to the expected field performance (Phase III).

Phase I of the project was completed. However, Phase II and Phase III were not carried out because the project was discontinued. Thus, this report only documents the pre-construction tests conducted by researchers on a scheduled overlay project along I-20 in the Atlanta District and the Phase II work plan developed by the researchers, project director, and program coordinator.

17. Key Words	18. Distribution Statement
Nondestructive Testing, Seismic Pavement Analyzer, Ground Penetrating Radar	No restrictions. This document is available to the public through NTIS: National Technical Information Service 5285 Port Royal Road Springfield, Virginia 22161

19. Security Classif.(of this report)	20. Security Classif.(of this page)	21. No. of Pages	22. Price
Unclassified	Unclassified	98	

PREDICTING HOT-MIX PERFORMANCE FROM MEASURED PROPERTIES: PHASE II PROJECT DOCUMENTATION

by

Emmanuel Fernando
Associate Research Engineer
Texas Transportation Institute

Tom Scullion
Research Engineer
Texas Transportation Institute

and

Soheil Nazarian
Professor of Civil Engineering
The University of Texas at El Paso

Report 0-1708-2
Project Number 0-1708
Research Project Title: Predicting Hot-Mix Performance from Measured Properties

Sponsored by the
Texas Department of Transportation
In Cooperation with the
U.S. Department of Transportation
Federal Highway Administration

November 2001

TEXAS TRANSPORTATION INSTITUTE
The Texas A&M University System
College Station, Texas 77843-3135

DISCLAIMER

The contents of this report reflect the views of the authors, who are responsible for the facts and the accuracy of the data presented herein. The contents do not necessarily reflect the official views or policies of the Texas Department of Transportation (TxDOT), or the Federal Highway Administration (FHWA). This report does not constitute a standard, specification, or regulation, nor is it intended for construction, bidding, or permit purposes. The engineers in charge of the project were Emmanuel G. Fernando, P.E. # 69614, and Tom Scullion, P.E. # 62683.

ACKNOWLEDGMENTS

The work reported herein was conducted as part of a research project sponsored by TxDOT and FHWA. Miles Garrison, and Dale Rand of TxDOT served as program coordinator, and project director, respectively.

TABLE OF CONTENTS

Page

LIST OF FIGURES

Figure Page

Figure Page

LIST OF TABLES

CHAPTER I
INTRODUCTION

Project 0-1708, "Predicting Hot-Mix Performance from Measured Properties," was initiated by the Texas Department of Transportation to develop simple, practical, and reliable test procedures for evaluating the quality of finished hot-mix asphalt concrete (HMAC) pavements on the basis of predicted performance. To accomplish this goal, the research project statement specified a three-phased work plan that called for:

- conducting a detailed review of recent and ongoing related studies at the state and federal level (Phase I);
- identifying mixture-, construction-, and structural-related properties that are significant predictors of pavement performance and are under the contractor's control (Phase II); and
- identifying/modifying existing procedures or developing new procedures that relate the properties from Phase II to the expected field performance (Phase III).

The research project statement recognized that achieving this goal is a complex undertaking and will require a long-term research effort that "*if successful, should result in performance models which can be used to determine, in a quantifiable manner, the impact of the contractor's operations and decisions on expected life of an HMAC pavement.*" Researchers completed Phase I of the project in the first year. The findings from this phase are documented in a research report (Fernando et al., 2000) that presented:

- a detailed review of the state-of-knowledge with respect to test methods for measuring construction quality indicators of relevance to the study,
- available models to establish the impact of the contractor's operations and decisions on expected performance, and
- a proposed work plan for Phase II and Phase III to develop rational and practical test methods for evaluating the quality of HMAC pavements.

During the second year, however, TxDOT changed the scope of the project to focus on establishing a database on in-service pavements for future evaluation and verification of

pavement performance models. For this purpose, the program coordinator identified a set of test sections in the Atlanta district that were to be built as part of a rehabilitation project along I-20 near Marshall, Texas. Researchers were asked to monitor this project before, during, and immediately after construction to establish a database of initial properties that may be used at a future time to evaluate relationships between observed field performance and initial as-built properties. A new work plan was subsequently developed, from joint discussions with the project director and program coordinator, that laid out the tests to be conducted in the monitoring effort and the properties that were to be measured and assembled into a database. Accordingly, the termination date of the project was also changed from August 2004 to August 2002, to coincide with the completion of construction work and testing along I-20.

However, the new work plan was never carried out. At the June 2001 Research Management Committee (RMC) meeting in Dallas, the RMC decided to terminate Project 0-1708 at the end of fiscal year 2001. As the actual construction of the HMAC test sections did not begin until September, none of the proposed tests in the work plan were conducted under this project. Thus, this final report documents only the following:

- results from ground penetrating radar (GPR) and seismic pavement analyzer (SPA) tests conducted by researchers on the existing pavement along I-20 prior to construction, and
- work plan developed by the researchers, project director, and program coordinator to measure initial properties of test sections along I-20 for future evaluation of field performance.

The results from the GPR and SPA tests are presented in Chapter II along with background material on these nondestructive test methods. Chapter III presents the work plan as formulated between the researchers, project director, and program coordinator. Finally, the appendices present tables and figures of the SPA and GPR test results.

CHAPTER II
SPA AND GPR TESTING ALONG I-20 PROJECT BEFORE CONSTRUCTION

SPA PRE-CONSTRUCTION TESTING

In March 2001, researchers from the University of Texas at El Paso conducted seismic pavement analyzer tests along four sections of I-20 near Marshall, Texas, to determine the variation in the moduli of the existing asphalt concrete pavement (ACP), qualify the condition of the Portland cement concrete pavement (PCCP) underneath the ACP, and estimate the support condition from the subgrade. The documentation of the SPA tests covers the following sections:

- description of the device: its applications, operation, strengths, and limitations;
- review of test methods;
- sections tested; and
- results from analysis of the test data collected by researchers.

Seismic Pavement Analyzer

The seismic pavement analyzer, shown in Figure 1, is an instrument designed to determine the variation in modulus with depth of pavement sections. With the SPA, pavement engineers can estimate shear and/or Young's modulus of different layers using one or all of the following methods:

- ultrasonic body waves (UBW),
- ultrasonic surface waves (USW),
- impulse response (IR),
- impact echo (IE), and
- spectral analysis of surface waves (SASW).

The SPA records the pavement response produced by high- and low-frequency pneumatic hammers on five accelerometers and three geophones. A computer controls data acquisition, instrument control, and interpretation. The quality of collected data is generally better than

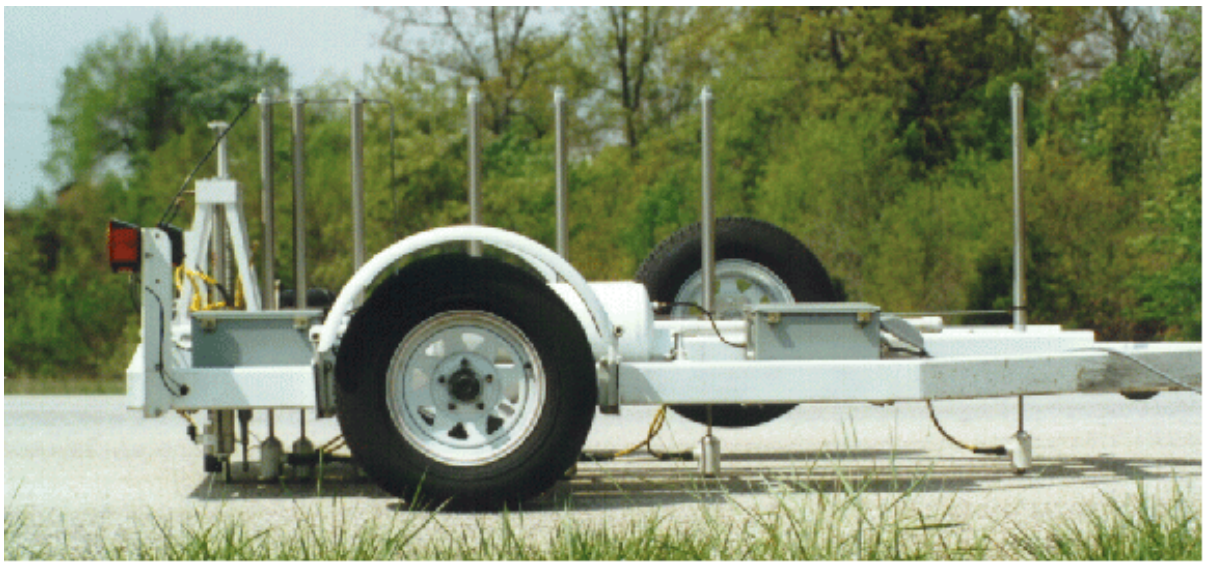

a) Device in Use

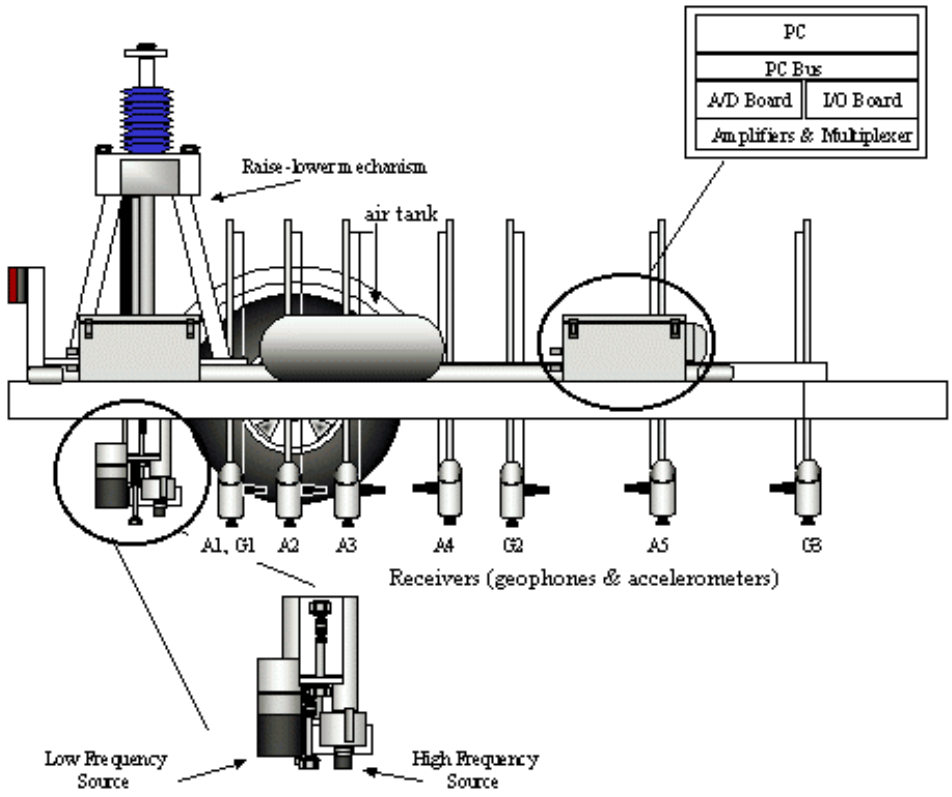

b) Schematic

Figure 1. The Seismic Pavement Analyzer.

those collected manually because a computer controls the operation of the source and receivers. The equipment has been used in several applications:

- analyzing, in detail, pavement conditions in project-level surveys;
- diagnosing specific distress precursors to aid in selecting a maintenance treatment; and
- monitoring pavement conditions after construction as a quality control tool.

The operating principle of the SPA is based on generating and detecting stress waves in a layered medium. Table 1 summarizes each of the five tests and its areas of strength and weaknesses. The design and construction of the SPA are based on two general principles. First, the strength of each method should be fully utilized; second, testing should provide enough redundancy to identify the properties of each layer within a pavement.

The ultrasonic body wave method can determine Young's modulus of the top pavement layer. Similarly, the ultrasonic surface wave method can be used to determine the shear modulus of the material. The impulse response method can be used to evaluate the condition of the support by measuring the stiffness of the slab at different locations. The impact echo method can be used to determine the overlay delamination or to measure the thickness of the top layer. Engineers can use the SASW method to determine the modulus and thickness of each layer in the pavement.

To collect data with the SPA, the technician initiates the testing sequence through the computer, which then lowers the sensors and impact unit onto the pavement surface. The high-frequency source is then activated. The outputs of the three accelerometers closest to the high-frequency source, as well as the load cell connected to this source, are used first. The source is fired four to seven times. For the last three impacts of the source, the output voltages of the load cell and the receivers are saved and averaged (stacked) in the frequency domain. The other (pre-recording) impacts are used to adjust the gains of the pre-amplifiers. The gains are set in a manner that optimizes the dynamic range. The same procedure is followed again, but the first three accelerometers are replaced by the last three accelerometers. The middle accelerometer (A3 in Figure 1) is active in both sets of experiments.

Typical voltage outputs of the load cell and the three near accelerometers are shown in Figure 2. To ensure that an adequate signal-to-noise ratio is achieved in all channels,

Table 1. Pavement Parameters Measured with Different Seismic Methods Used in SPA.

Method	Primary Use	Strengths	Weaknesses
Ultrasonic Body Waves	Modulus of top layer	• Rapid to perform • Simple data reduction	• Results may be affected by underlying layers • Sensitive to surface condition
Ultrasonic Surface Waves	Modulus of top layer	• Sensitive to properties of top layer • Rapid to perform • Layer specific results	• For multi-course pavements, determination of layer-specific information is complex
Impact Echo	Thickness of top layer or depth to delaminated interface	• Can determine thickness of the layer • Sensitive to delaminated interfaces	• Substantial contrast between the modulus of two adjacent layers is needed for sensitivity • For multi-course pavements, at least one core is needed for calibration • Applies only to pavements with thicker top layer
Impulse Response	Modulus of subgrade reaction of foundation layers or overall modulus of a pavement	• Powerful tool for rapidly locating weak spots in a pavement • May be used to estimate depth to stiff layer (in progress)	• For flexible pavements, the contribution of different layers are unknown • Results are affected by depth to rigid layer and water table
Spectral Analysis of Surface Waves	Modulus and thickness of each layer	• Provides the modulus profile in a comprehensive manner • More robust than deflection-based methods	• Data reduction is time consuming and complex • Automated analysis applicable only to simple structures

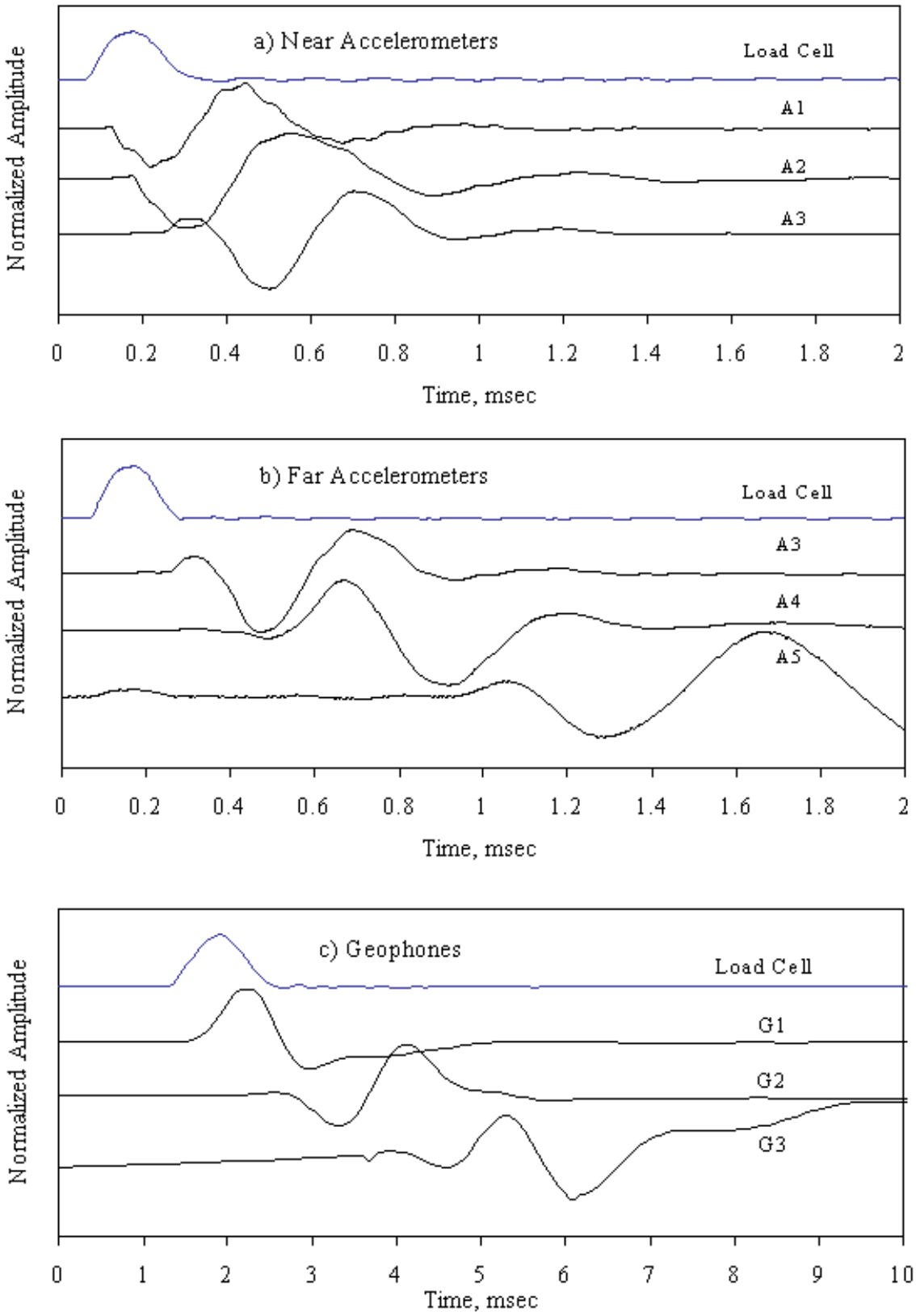

Figure 2. Typical Time Records from SPA.

signals are normalized to maximum amplitude of one. In this manner, the main features of the signals can be easily inspected.

In the next phase of data collection, the data from the low-frequency load cell and the three geophones are recorded. The procedure described above for each of the accelerometer banks is utilized. A typical output of the three geophones is also shown in Figure 2 in the normalized fashion. The data collected are processed using signal processing and spectral analysis. Data processing for each of the five tests is described in the next section.

Description of Measurement Technologies

Impulse Response Method

The goal of the impulse response method is to determine the overall stiffness of a pavement section. The overall stiffness can be correlated to the modulus of subgrade reaction for rigid pavements or to an effective modulus for flexible pavement. Figure 3 shows a schematic of the IR method. For this test, the low-frequency source and geophone G1 (see Figure 1) are used. The pavement is impacted to couple stress wave energy in the surface layer. The imparted energy, denoted as F(t) in Figure 3, is measured with a load cell, and the response of the pavement, in terms of displacement *(t), is monitored with the geophone [1]. The load and displacement time-histories are simultaneously recorded and are transformed to the frequency domain using a fast-Fourier transform algorithm. At each frequency, the ratio of the load and displacement, termed stiffness, is then determined.

A comprehensive numerical and experimental study by Reddy (1992) demonstrated that, for both rigid and flexible pavements, the stiffness spectrum (variation in stiffness with frequency) quite reasonably resembles the response of a single-degree-of-freedom (SDOF) system. Three parameters numerically describe a SDOF system. In our case, these parameters are the static stiffness (stiffness at a frequency of 0 Hz), a damping ratio, and a natural frequency.

---

[1] Geophones actually measure particle velocity, but the data can be transformed to deflection using appropriate signal analysis procedure. See Nazarian and Bush (1990) for a comprehensive description of the methodology.

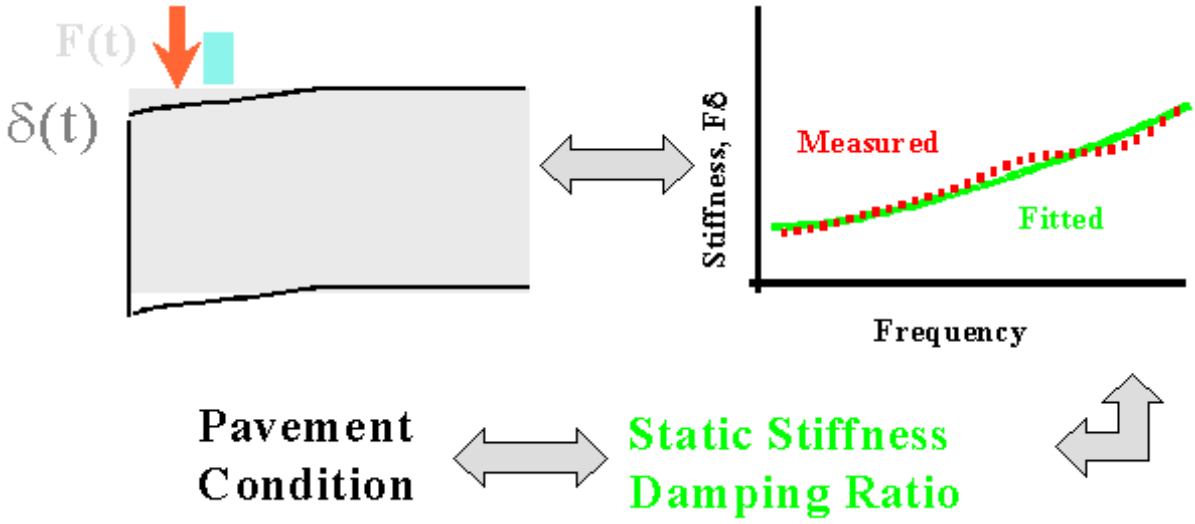

Figure 3. Schematic of Impulse Response Test Method.

The static stiffness can be physically related to an overall modulus of the pavement system. For intact rigid pavements where the PCCP is much stiffer than the subgrade, the overall modulus can be related to the modulus of subgrade reaction provided the dimensions of the slab, the modulus of PCCP, and the location of impact are known (Nazarian et al., 1994). On the other hand, the overall modulus measured on a flexible pavement is significantly influenced by the modulus and thickness of the upper layers and, hence, cannot be readily related to the modulus of subgrade. For rigid pavements with weak support or loss of support, the overall stiffness will significantly decrease. In these cases, the damping ratio can distinguish between the loss of support or weak support. The natural frequency is related to the extent of loss of support. However, further research is required to develop such a relationship.

Reddy (1992) describes the procedure to quantify the relationships described above. Briefly, as shown in Figure 3, a curve is fitted to the stiffness to determine the modal parameters. The modulus of subgrade, E_{sg}, is calculated from:

$$E_{sg} = \frac{2(1+n)(1-n)S_0}{2LI_sS_z} \quad (1)$$

where,

$<$ = Poisson's ratio of subgrade,

L = length of slab,

S_0 = static stiffness of slab (stiffness at a frequency of 0 Hz),

S_z = shape factor, and

I_s = flexibility parameter.

Dobry and Gazetas (1986) have developed the shape factor, Sz. I_s (Nazarian et al., 1994) is a parameter which considers the effect of an increase in flexibility near the edges and corners of a slab. Parameter I_s is a function of the length and width of the slab, as well as the coordinates of the impact point relative to one corner. Depending on the size of the slab and the point of impact, the value of I_s can be as high as six.

The damping ratio for PCCP slabs, which typically varies between 0 to 100 percent, is an indicator of the degree of the slab's resistance to movement. A slab that is in contact with the subgrade or contains a water-saturated void demonstrates a highly damped behavior and has a damping ratio of greater than 70 percent. A slab containing an edge void would demonstrate a damping ratio on the order of 10 to 40 percent. A loss of support located in the middle of the slab will have a damping of 30 to 60 percent. For ACP, the damping ratio is usually greater than 70 percent.

As indicated before, engineers can effectively use the impulse response method to determine the overall stiffness of the system and, as such, is a robust indicator of the health of the pavement. McDaniel et al. (1999) demonstrated that there is a trend between the modulus of subgrade determined by the IR method and the deflection of sensors 1 and/or 2 of the falling weight deflectometer (FWD).

Spectral Analysis of Surface Waves Method

The spectral analysis of surface waves method is a seismic method that can provide modulus profiles of pavement sections nondestructively. Since a large number of published reports and papers are available on this topic, only a brief description is included here. The key point in the SASW method is the measurement of the dispersive nature of surface waves. A complete investigation of a site with the SASW method consists of collecting data,

determining the experimental dispersion curve, and determining the stiffness profile (inversion process).

With the current SPA sensor configuration, the determination of an accurate modulus of subgrade from the SASW method under a PCCP is doubtful. This problem can be readily resolved by incorporating longer receiver spacings in the SPA. Also, since the layering is determined from the contrast in moduli of two adjacent layers, the accurate determination of the boundary of two layers with similar stiffness is difficult. However, the combined thickness of the two layers is estimated reasonably well.

Ultrasonic Surface Wave Method

The ultrasonic surface wave method[2] is an offshoot of the SASW method. The major distinction between these two methods is that in the ultrasonic-surface-wave method the modulus of the top pavement layer can be directly determined without an inversion algorithm. To implement the method, the high-frequency source and accelerometers A2 and A3 or A3 and A4 of the SPA (see Figure 1) are utilized.

As sketched in Figure 4, at wavelengths less than or equal to the thickness of the uppermost layer, the velocity of propagation is independent of wavelength. Therefore, if one simply generates high-frequency (short-wavelength) waves, and if one assumes that the properties of the uppermost layer are uniform, the shear wave velocity of the upper layer, V_s, can be determined from:

$$V_s = \left(1.13 \quad 0.16n\right)V_{ph} \tag{2}$$

where V_{ph} is the velocity of surface waves. The modulus of the top layer, E_t, can be determined from:

$$E_t = 2\,r\;V_s^{\,2}\left(1+n\right) \tag{3}$$

---

[2] Some organizations involved in seismic tests do not differentiate between the USW and the SASW methods. In our terminology, the SASW test is a comprehensive test that requires the development of an experimental dispersion curve and determining the modulus profile through an inversion process. The USW simply provides the modulus of the top layer without need for an inversion process and, as such, is much simpler to perform.

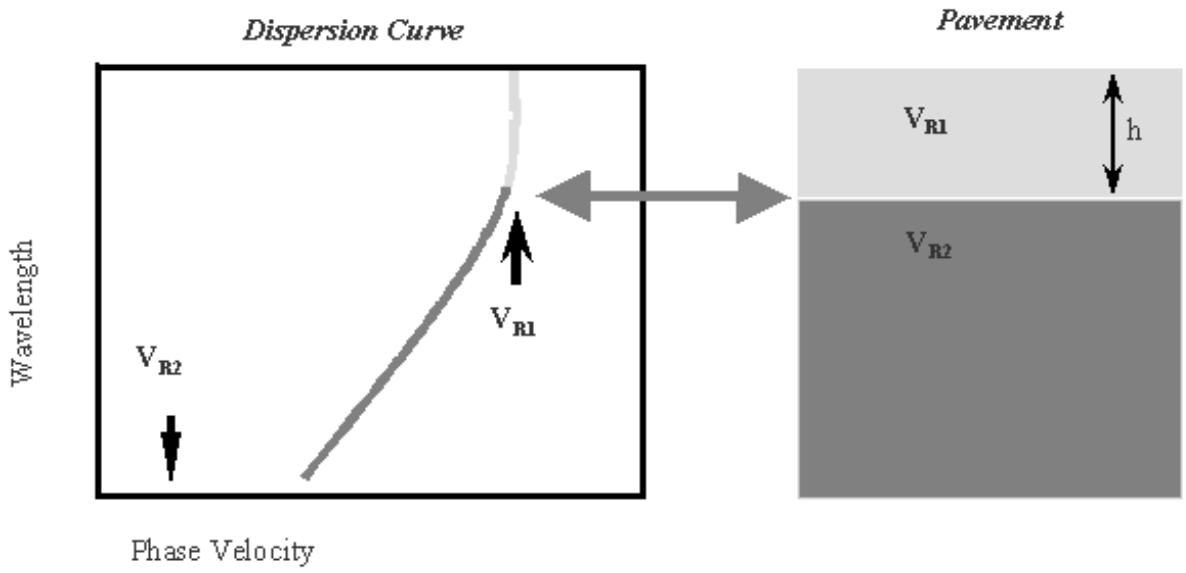

Figure 4. Schematic of USW Method.

where ρ is the mass density. The wavelength at which the phase velocity is no longer constant is closely related to the thickness of the top layer (NCHRP, 1996).

Ultrasonic Body Wave Method

Theoretically, all accelerometers can be used to measure compression, shear, or surface wave velocity of the upper layer of pavement. A typical record is shown in Figure 5. Once the wave velocity of a material is known, its Young's modulus can be readily determined.

In the ultrasonic body wave analysis, one relies on identifying the time at which different types of energy arrive at each sensor. The velocity of propagation, V, is typically determined by dividing the distance between two receivers, ΔX, by the difference in the arrival time of a specific wave, Δt. In general, the relationship can be written in the following form:

$$V = \frac{X}{t} \tag{4}$$

In the equation, V can be the propagation velocity of any of the three waves [i.e. compression wave, V_P; shear wave, V_S; or surface (Rayleigh) wave, V_R]. Knowing wave velocity, modulus

can be determined in several ways. Young's modulus, E, can be determined from shear modulus, G, and Poisson's ratio, <, using:

$$E = 2(1+n)G \tag{5}$$

Shear modulus can be determined from shear wave velocity, V_s, using:

$$G = \frac{g}{g} V_s^2 \tag{6}$$

To obtain modulus from surface wave velocity, V_R is first converted to shear wave velocity using:

$$V_s = V_R(1.13 \quad 0.16n) \tag{7}$$

The shear modulus is then determined from Eq. (6).

Figure 5 shows a typical record from a sensor. As an example, the arrivals of compression, shear and surface waves are marked on the figure. The compression wave (or P-wave) energy is reasonably easy to identify because it is the earliest source of energy to appear in the time record. Since less than 10 percent of the seismic energy propagates in this form, the peak compression wave energy in the signal sometimes is only several times above the inherent background noise. This limitation may make it difficult to always reliably estimate the arrivals of these waves, especially on thin ACP.

The shear wave (or S-wave) energy is about one-fourth of the seismic energy and, as such, is better pronounced in the record. The practical problem with identifying this type of wave is that it propagates at a speed that is close to that of the surface waves. As such, the separation of the two energies, at least for short distances from the source, may be difficult.

Surface (Rayleigh) waves contain about two-thirds of the seismic energy. As marked in Figure 5, the most dominant arrivals are related to the surface waves; as such, it should be easy to measure them. If a layer does not have surface imperfections, and if the impact is sharp enough to generate only waves that contain energy for wavelengths shorter than the thickness of the top layer, one can readily use this method to determine the modulus. However, it may be difficult to observe these two restrictions. The USW method, even though more complex to implement, is by far more robust than the UBW analysis.

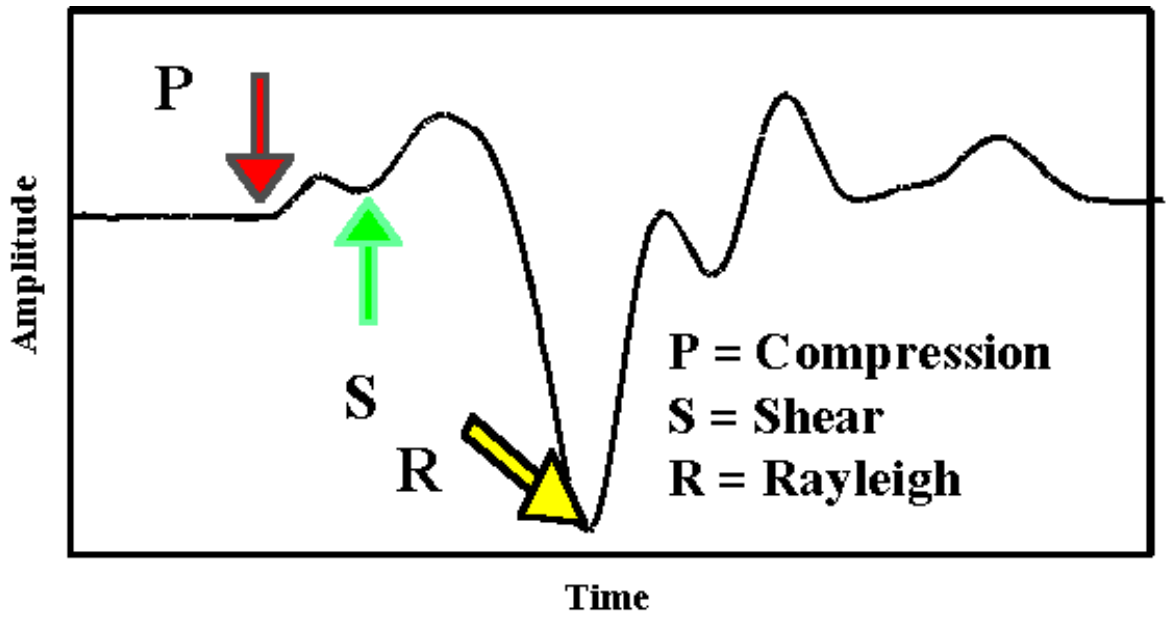

Figure 5. Typical Time Record Used in UBW Method.

Impact Echo Method

The impact echo method can effectively locate defects, voids, cracks, and zones of deterioration within concrete. This method has been thoroughly studied and effectively used on many projects by researchers at the National Institute of Standards and Technology (Sansalone and Carino, 1986).

The high-frequency source and accelerometer A1 or A2 of the SPA are typically used (see Figure 1). The method, as sketched in Figure 6, is based on detecting the frequency of the standing wave reflecting from the bottom and the top of the top pavement layer. Upon impact, some of the energy is reflected from the bottom of the layer, and some is transmitted into the base and subgrade. Since the top of the layer is in contact with air, almost all of the energy is reflected from that interface. The receiver senses the reflected energy at periodic intervals. The period depends on the thickness and compression wave of the layer. To conveniently determine the frequency associated with the periodic arrival of the signal, one can utilize a fast-Fourier transform algorithm. The frequency associated with the reflected wave appears as a peak in the amplitude spectrum. Once the compression wave velocity of concrete, V_p, is known, the depth-to-reflector, h, can be determined from:

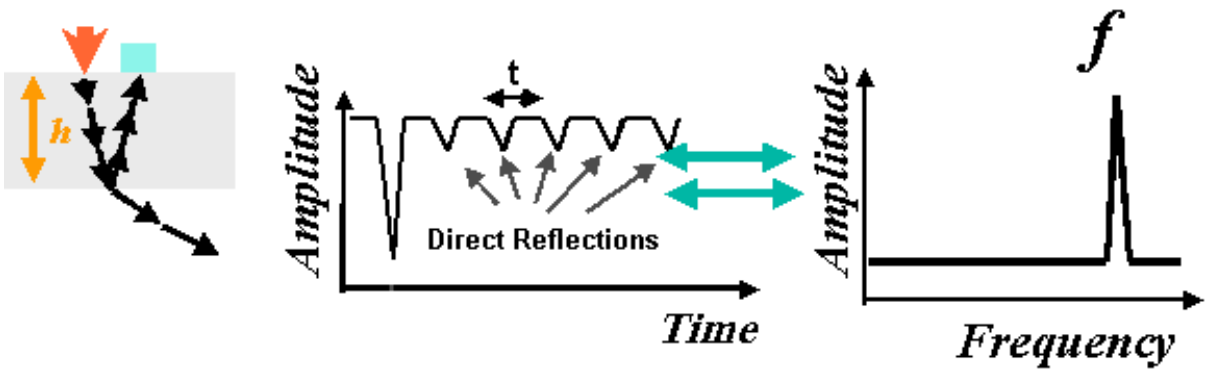

Figure 6. Schematic of Impact Echo Method.

$$h = \frac{V_p}{2f} \tag{8}$$

where f is the resonant frequency obtained by transforming the deformation record into the frequency domain. One can determine the compression wave velocity if the surface wave velocity is known from:

$$V_p = \frac{V_R \left(1 \quad n\right)^{0.5}}{\left(0.5 \quad n\right)^{0.5} \left(1.13 \quad 0.16n\right)} \tag{9}$$

As detailed in Nazarian et al. (1997), the method is not applicable to relatively thin layers and layers where the difference in moduli of adjacent layers is small. Even though the method has been used extensively in concrete, the use of the IE method on ACP and composite profiles is fairly new. Several elements indicate that a core or two are needed to calibrate the results when the method is used in these conditions. Unlike concrete, in which the in-place material is homogeneous, thick asphalt concrete (AC) layers are usually placed and compacted in several lifts, often with different mixtures. Therefore, it is difficult to ensure vertical homogeneity. Second, the variation in temperature with depth results in a vertically heterogeneous material. Third, the large damping properties of the material make it difficult to detect the arrival of the compression waves. In this case, a Poisson's ratio has to be assumed.

Description of Site

Tests were carried out along the east- and west-bound sections of the I-20 overlay project limits. Both the inside and outside lanes were tested at intervals of approximately 100 ft. The cross-sectional profile of the site, which was similar for the west- and east-bound, consisted of a micro-surfacing layer over approximately 4 inches of AC, over about 8 inches of continuously reinforced concrete pavement (CRCP). The supporting layers consisted of about 7 inches of cement-stabilized base over approximately 6 inches of cement-treated subbase over 6 inches of select material.

Analysis of Test Data

The two primary seismic test methods used in this project were IR and USW. As indicated before, the current set-up of the SPA is not suitable for SASW tests on rigid pavements.

Several problems within and beneath the pavement layers are possible. These include:

- low-quality ACP (low modulus or high air-void content),
- debonded ACP (separation of AC from underlying concrete),
- low-quality PCCP (low modulus, badly damaged or cracked concrete),
- void under the slab, and
- soft support.

In non-uniform and complex sites conditions, such as the one here, nondestructive testing should be supplemented with coring and other site investigation tools. Unfortunately, due to time limitation this was not carried out.

AC Layer

Researchers determined the seismic moduli of the ACP at numerous points using the USW method as discussed above. For this purpose, the records from accelerometers 2 and 3 were used. The point-by-point results can be found in Appendix A.

Figure 7 shows the variations in the AC modulus with station numbers for the eastbound and the westbound lanes. The temperature varied from site to site and from location to location. The average temperature measured at each site was used to adjust the

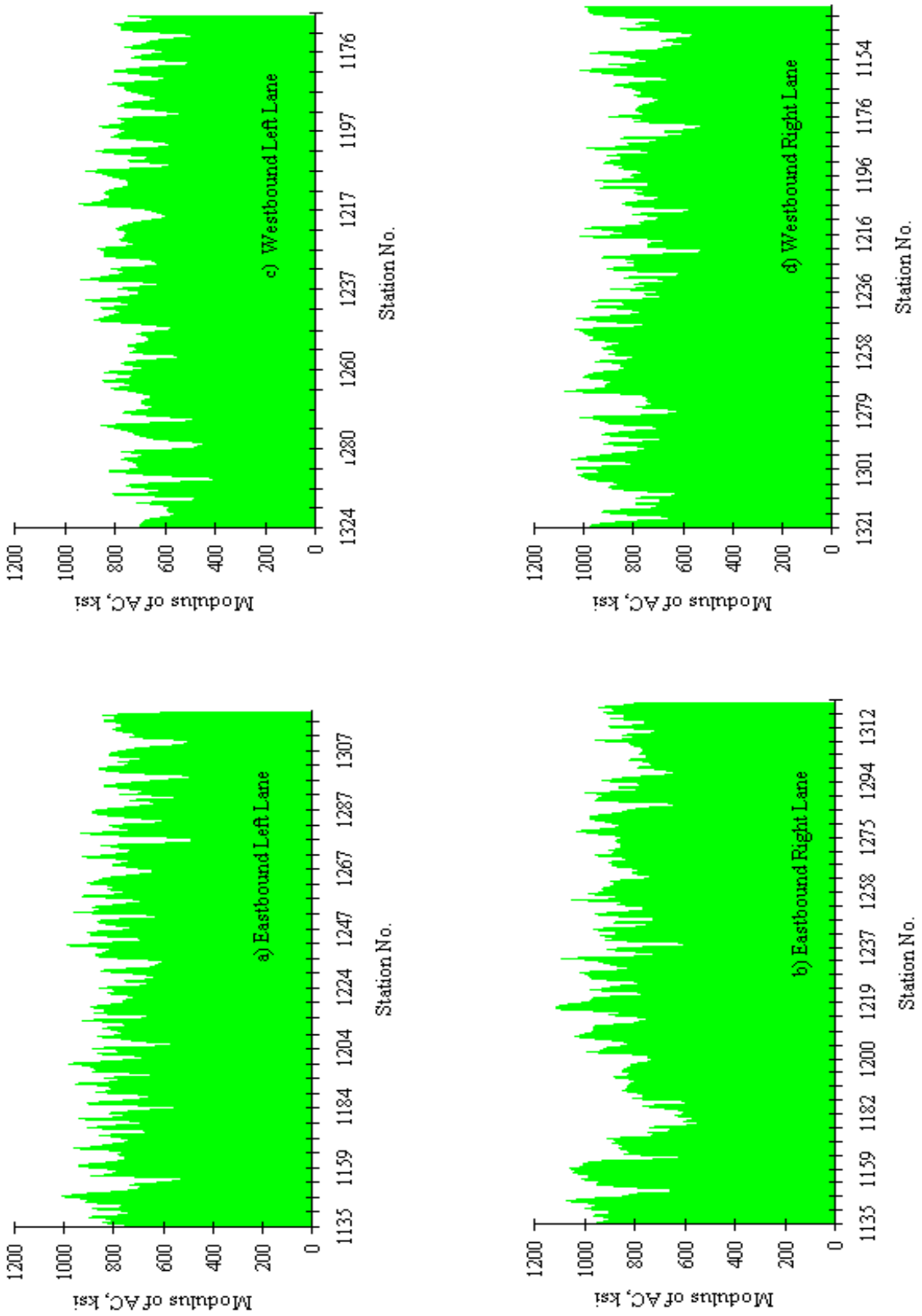

Figure 7. Predicted Variation in AC Modulus along I-20 Project.

AC moduli to 25 °C (77 °F). The relationship suggested by Li and Nazarian (1994) for such adjustment was used here. That relationship is:

$$E_{25} = \frac{E_T}{1.35 \quad 0.014\,T} \tag{10}$$

where,

E_{25} = AC modulus corrected to 25 °C; and

E_T = AC modulus at test temperature, T, in °C.

The AC moduli measured with seismic methods in general and the SPA in particular are low-strain high-frequency moduli. To adjust the AC moduli to frequency and strain levels similar to those measured with the FWD, Aouad et al. (1993) proposed that the seismic modulus at 25 °C (77 °F) be divided by a factor of about 3. The AC moduli reported in this chapter are adjusted for both temperature and strain-rate. The results are summarized in Table 2. On the average, the ACP layer seems to be stiff with an average modulus of more than 750 ksi. This may be because the ACP is high quality or because it has stiffened due to aging. It should be mentioned that cracks were avoided during the tests. Typically, the existence of a crack between the two receivers results in unrealistically high or low moduli.

PCC Layer

The current configuration of the SPA does not allow for implementing the SASW method on rigid pavements. Because the longest sensor spacing for the SPA is 4 ft, a dispersion curve with long enough wavelengths to obtain reliable moduli is not possible. Researchers attempted to determine the quality of the concrete underlying the ACP indirectly.

Figure 8 contains the theoretical simulation of a dispersion curve that should have been observed at this site. Researchers attempted to approximate the modulus of the concrete by finding the average velocity from sensors A3 and A4 (see Figure 1) over the range of wavelengths of 180 mm to 280 mm. Based on Figure 8, the average velocity in this range should be greater than the average velocity of the ACP measured with the USW method using Sensors A2 and A3. The ratio of the velocity of the PCC to the velocity of the AC should be about 1.25.

Table 2. Statistics on Predicted AC Modulus from USW Method.

Direction	Lane	Statistics		
		Average (ksi)	Standard Deviation (ksi)	Coefficient of Variation (percent)
Eastbound	Left	786	124	16
	Right	864	124	14
Westbound	Left	832	136	16
	Right	726	117	16

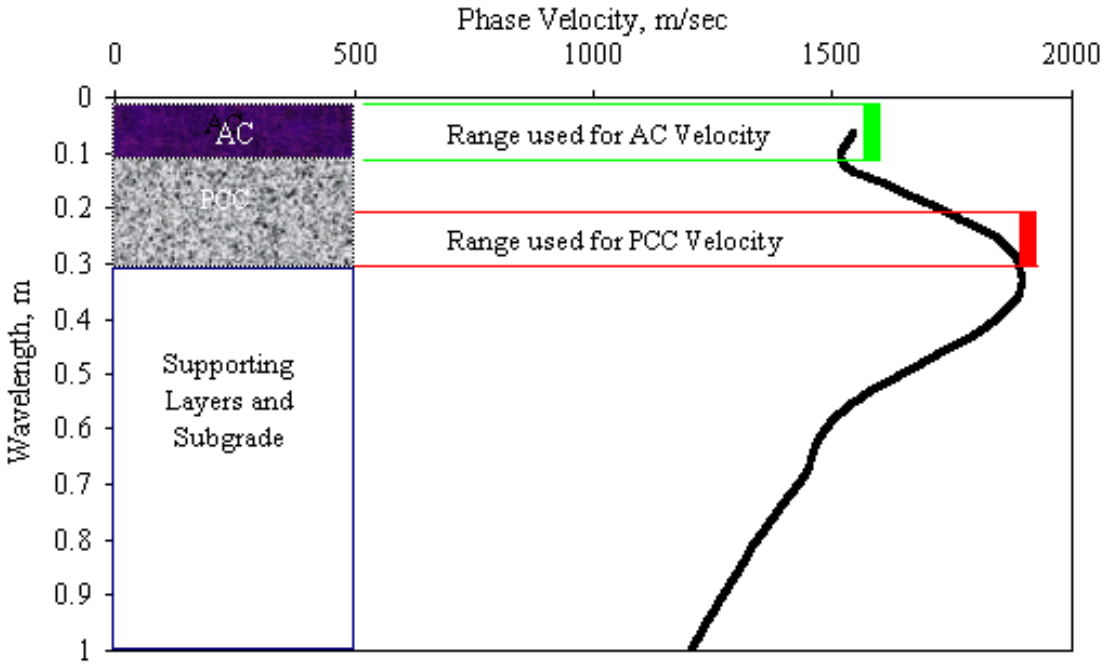

Figure 8. Typical Dispersion Curve from an Intact Cross-Section.

The variations in velocity ratio along the sections tested are shown in Figure 9. In most cases, the velocity ratio is less than one indicating that the approximate velocity of the concrete was less than that of the overlying AC layer. Two possible indications of velocity ratios below one are:

- the concrete is damaged, cracked, or is of extremely low quality; and
- the ACP layer is debonded from the PCCP to some varying degree.

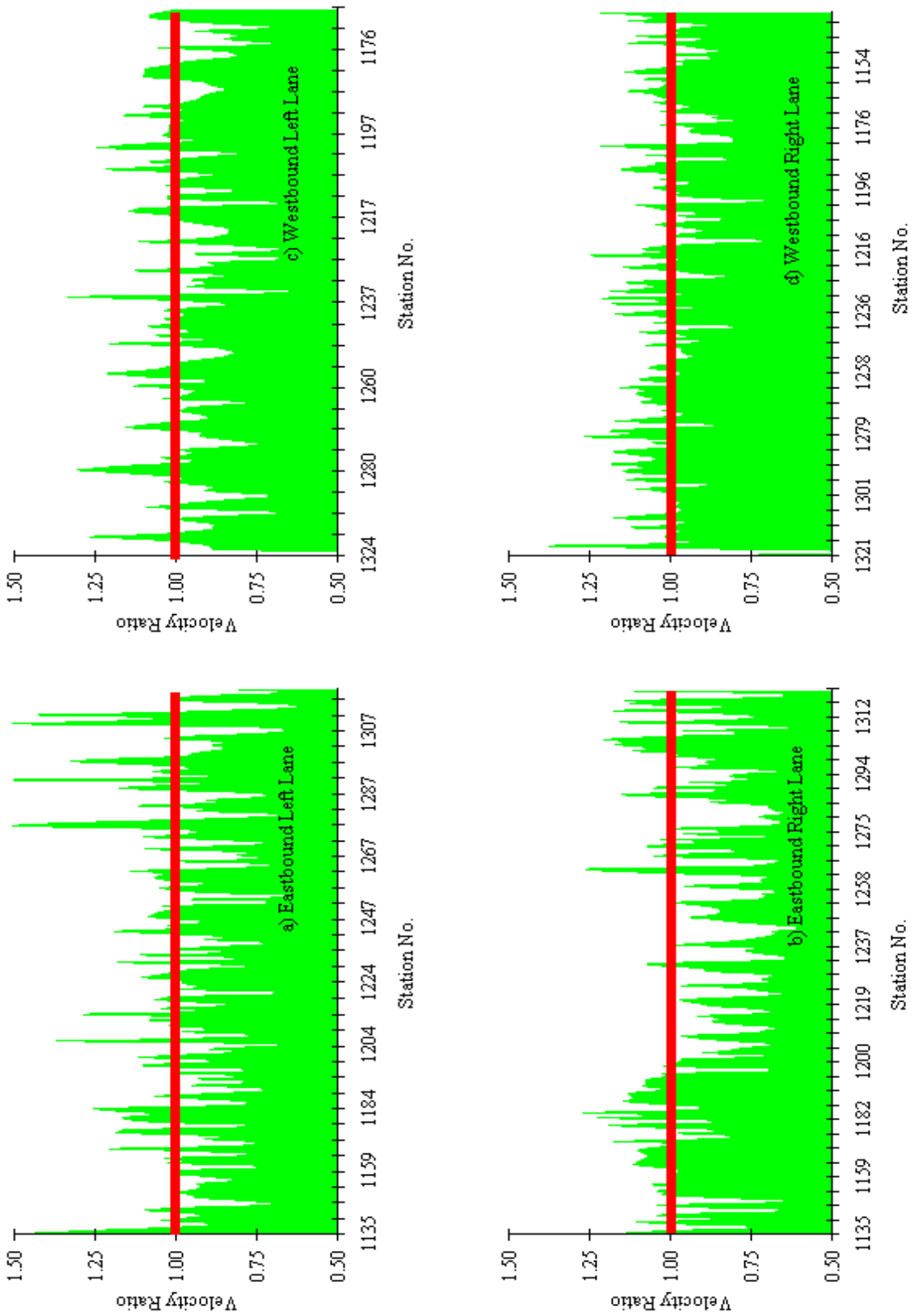

Figure 9. Variation in Velocity Ratio along the Project.

From the results, the most critical layer appears to be the right lane along the eastbound direction.

Composite Modulus of Subgrade

Researchers determined the composite modulus of subgrade using the IR method. Figure 10 shows the variation in composite modulus along the project. The values are extremely variable along the project indicating weak areas along the project. Table 3 summarizes the results from the IR tests.

In many cases, the composite moduli are rather small. Special attention should be paid to the westbound lanes. The low average composite moduli can be interpreted in two ways:

- The ACP is debonded from the PCC.
- The subgrade is very soft or voids exist between the PCC and underlying layers.

Coring is needed to verify the results from the SPA tests.

GPR PRE-CONSTRUCTION TESTING

Operational Principles of Ground Penetrating Radar

Figure 11 shows the one GHz air-launched GPR unit of the Texas Transportation Institute (TTI). This system sends discrete pulses of radar energy into the pavement system and captures the reflections from each layer interface within the structure. Radar is an electro-magnetic (EM) wave and therefore obeys the laws governing reflection and transmission of EM waves in layered media. This particular GPR unit can operate at highway speeds (55 mph), transmit and receive 50 pulses per second, and can effectively penetrate to a depth of 24 inches. A typical plot of captured reflected energy versus time for one pulse is shown in Figure 12 as a graph of amplitude in volts versus arrival time in nanoseconds.

The reflection, A_1, is the energy reflected from the surface of the pavement, and A_2 and A_3 are reflections from the top of the base and subgrade respectively. These are all illustrated as positive reflections, which indicate an interface with a transition from a low to a high dielectric material. As described later, these amplitudes of reflection and the time delays

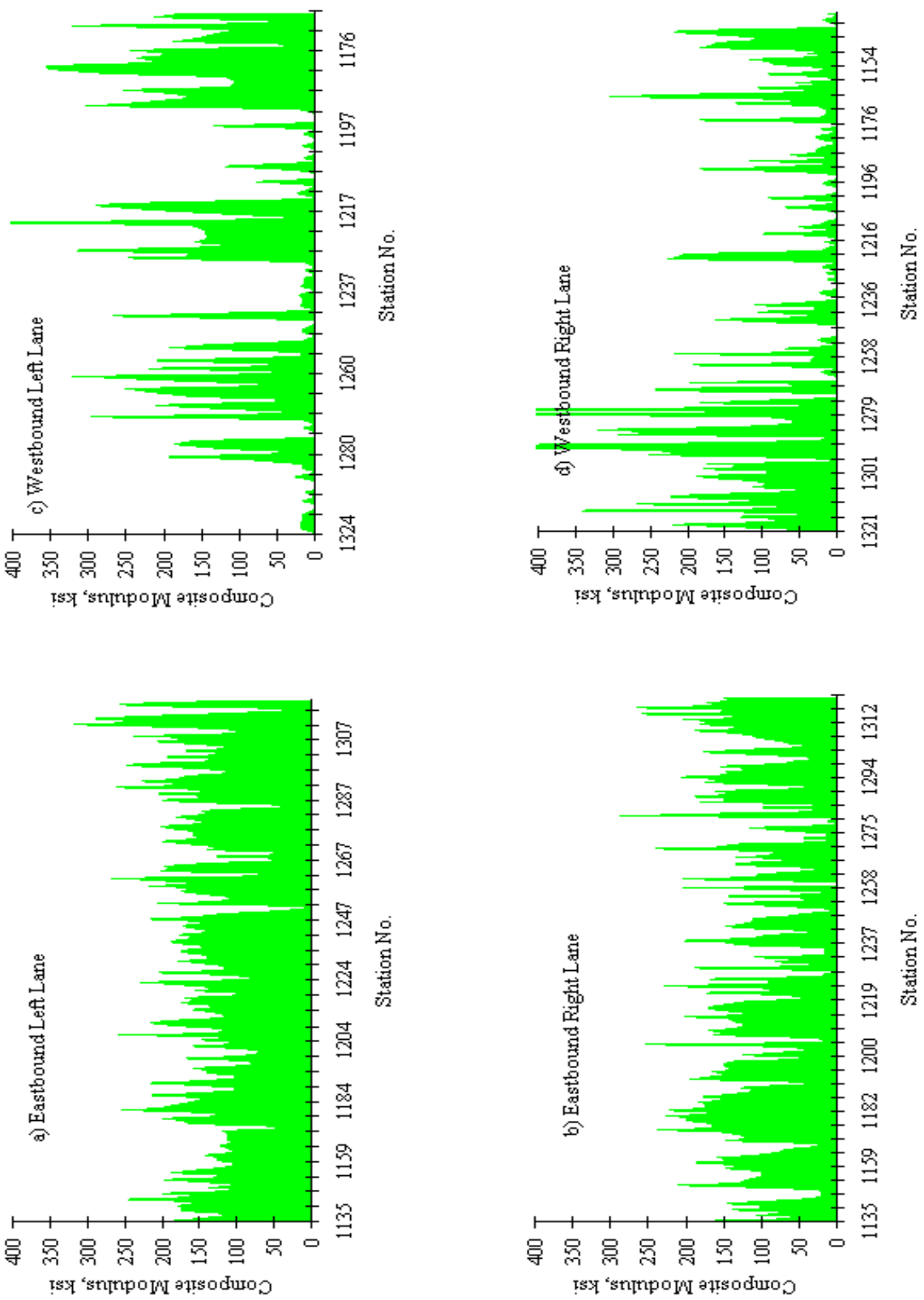

Figure 10. Variation in Composite Modulus along Project.

Table 3. Statistics on Predicted Composite Modulus of Subgrade.

Direction	Lane	Statistics		
		Average (ksi)	Standard Deviation (ksi)	Coefficient of Variation (percent)
Eastbound	Left	158	58	36
	Right	130	68	53
Westbound	Left	132	116	88
	Right	127	149	117

Figure 11. GPR Unit Used for Testing.

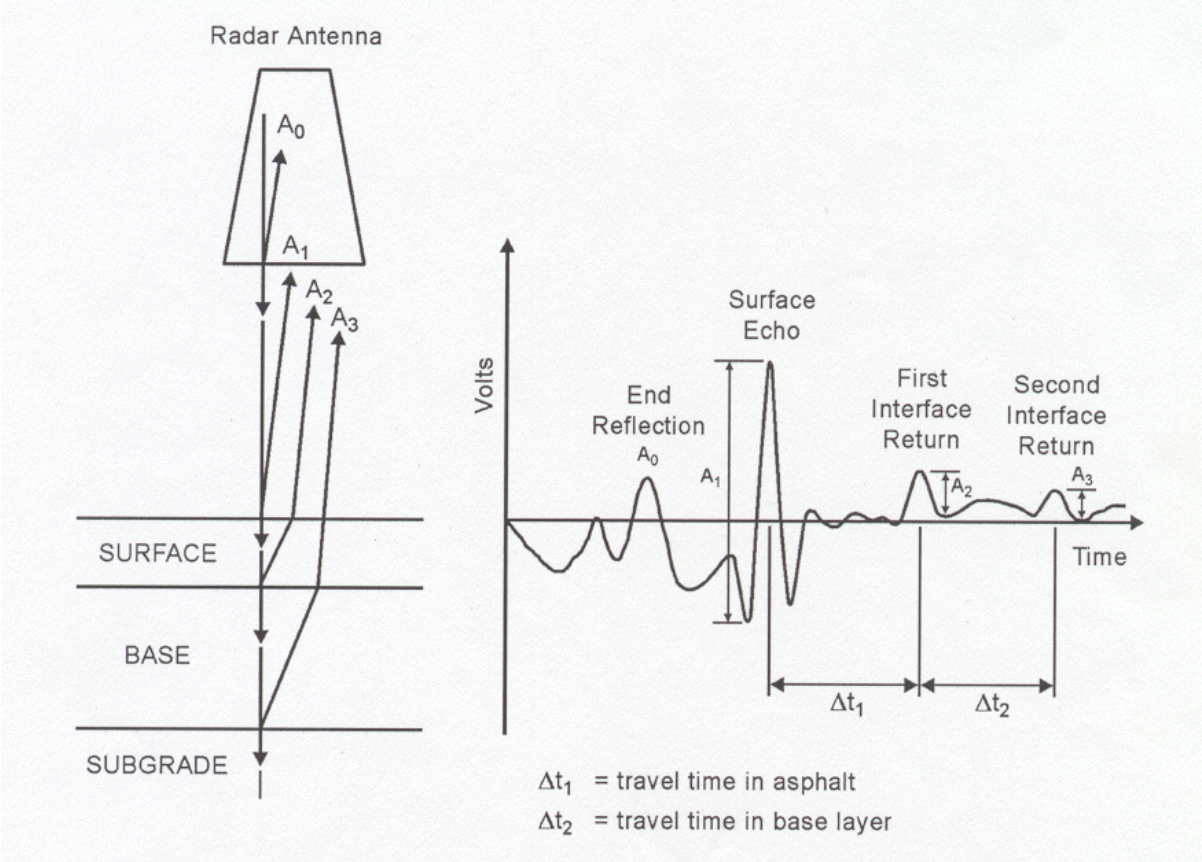

Figure 12. Illustration of Reflections from GPR Trace.

between reflections are used to calculate both layer dielectrics and thickness. The dielectric constant of a material is an electrical property which is most influenced by moisture content and density. An increase in moisture will cause an increase in layer dielectric. In contrast an increase in air void content will cause a decrease in layer dielectric.

A range of typical dielectrics has been established for most paving materials. Hot-mix asphalt (HMA) layers normally have a dielectric value between 4.5 and 6.5, depending on the coarse aggregate type. Measured values significantly higher than this would indicate the presence of excessive moisture. Lower values could indicate a density problem or indicate that an unusual material, such as lightweight aggregate, has been used. The examples below illustrate how changes in the pavement's engineering properties would influence the typical GPR trace shown in Figure 12:

- If the thickness of the surface layer increases, then the time interval between A_1 and A_2 would increase.
- If the base layer becomes wetter, then the amplitude of reflection from the top of the base, A_2, would increase.
- If there is a significant defect within the surface layer, then an additional reflection will be observed between A_1 and A_2.
- Large changes in the surface reflection, A_1, would indicate changes in either the density or moisture content along the section.

Layer Thickness Calculation

Using the amplitudes (volts) and time delays (ns) from Figure 12, it is possible to calculate layer dielectrics and layer thickness. The equations used are summarized below:

$$_{a} = \frac{1 + A_1 / A_m}{1 \quad A_1 / A_m}^{2} \tag{11}$$

where,

$,_a$ = the dielectric of the surfacing layer;

A_1 = the amplitude of surface reflection; and

A_m = the amplitude of reflection from a large metal plate in volts (this represents the 100 percent reflection case).

$$h_1 = \frac{5.9 \quad D\, t_1}{\sqrt{\quad_a}} \tag{12}$$

where,

h_1 = the thickness of the top layer; and

$) t_1$ = the time delay between peaks, A_1 and A_2.

$$\sqrt{\varepsilon_b} = \sqrt{\varepsilon_a}\,\frac{1 + \left(\frac{A_1}{A_m} + \frac{A_2}{A_m}\right)^2}{1 - \left(\frac{A_1}{A_2}\right)^2 \left(\frac{A_2}{A_m}\right)^2} \tag{13}$$

where,

ε_b = base dielectric; and

A_2 = the amplitude of reflection from the top of the base layer.

$$h_{base} = \frac{5.9 \times \Delta t_2}{\sqrt{\varepsilon_b}} \tag{14}$$

where,

h_{base} = thickness of base layer; and

Δt_2 = time delay between A_2 and A_3.

Using the above equations, one may calculate both layer thickness and dielectrics along the pavement. The use of the thickness information for either quality control of new construction or structural evaluation of existing structures is obvious to pavement engineers. However, the layer dielectric values and their variation along a highway are also of practical significance, as demonstrated by Saarenketo and Scullion (1995) and by Saarenketo (1996).

Results from GPR Testing

TTI researchers collected air-launched GPR data on the limits of the I-20 overlay project to document existing conditions and to provide information to personnel from the Materials and Pavements section who were performing tests with the Rolling Deflectometer. GPR testing was completed on April 2, 2001. The limits of the data collection were Texas reference markers (TRM) 610 to 614. Data were collected at one-foot intervals in both inside and outside lanes in both directions. A video of surface condition was also taken. The

researchers forwarded copies of the data files and the survey video to Dr. Michael Murphy of the Materials and Pavements section to assist with his interpretation of the Rolling Deflectometer data. Examples of pre-construction GPR data are shown in Figures 13 to 16. Color-coded representations of the GPR data on all lanes surveyed are given in Appendix B. Figures 13 to 16 show representative data taken on both directions. These are discussed in the following sections.

Eastbound Outside Lane – Outside Wheel Path

Figure 13 is a representative COLORMAP (Scullion and Chen, 1999) display from the eastbound lanes, taken from TRM 613 + 0.5 to 613 + 0.67. Similar data were obtained for much of the eastbound direction. At this location, the surfacing consists of two 2-inch thick lifts of asphalt concrete. The dielectric of the upper layer is relatively low at around 4.2 and 4.5. A strong reflection is observed at the top of the second layer of AC. The dielectric of the lower asphalt layer appears normal, in the range of 5.5 to 6. In several locations, full depth AC patches have been placed on this lane. These are clearly visible in the video as light colored patches. The dielectric values of these patches are close to 6, which is normal for AC.

It is also possible to identify the bottom of the PCC slab in Figure 13. A faint reflection is also observed from the middle of the PCC slab. The periodic, slightly brighter reflections could be from tie bars in the joints.

Westbound Outside Lane – Outside Wheel Path

The GPR images from the westbound direction were similar to those obtained in the eastbound direction. The total AC thickness is close to 4 inches. However more patches have been placed on this lane, and the pavement structure is more variable. This observation is illustrated in Figure 14 which shows a section from TRM 611 – 0.3 to 611 – 0.6. In section 1, the original AC layers have been removed and replaced with a single homogeneous layer. Section 2 shows a different GPR display. In this section, periodic low density areas are found in the lower AC layer, denoted by the blue areas in Figure 14. These could be areas of stripping in the lower AC layer, or they could be areas where the dense AC layer has been replaced with a drainable layer.

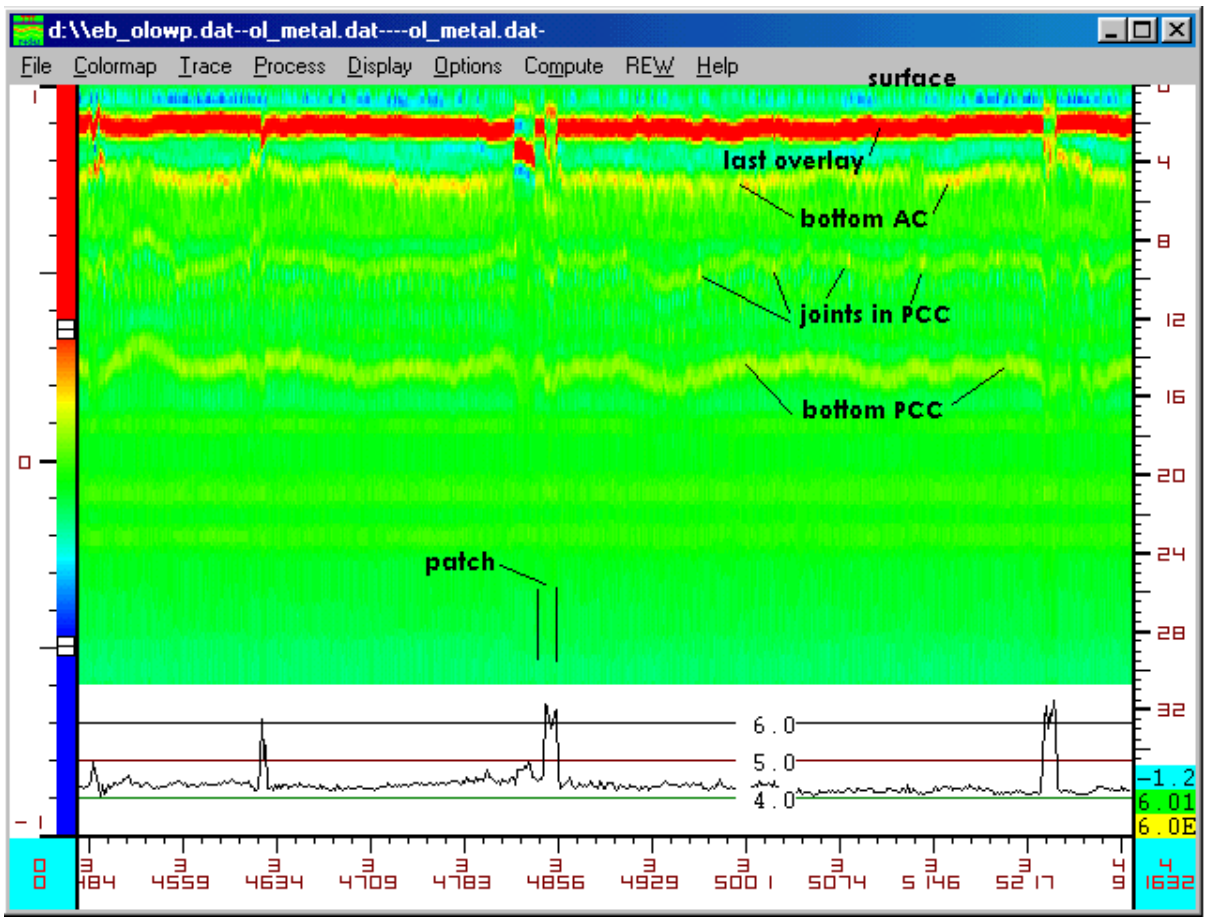

Figure 13. Typical COLORMAP Display from a Representative Area in the Eastbound Direction.

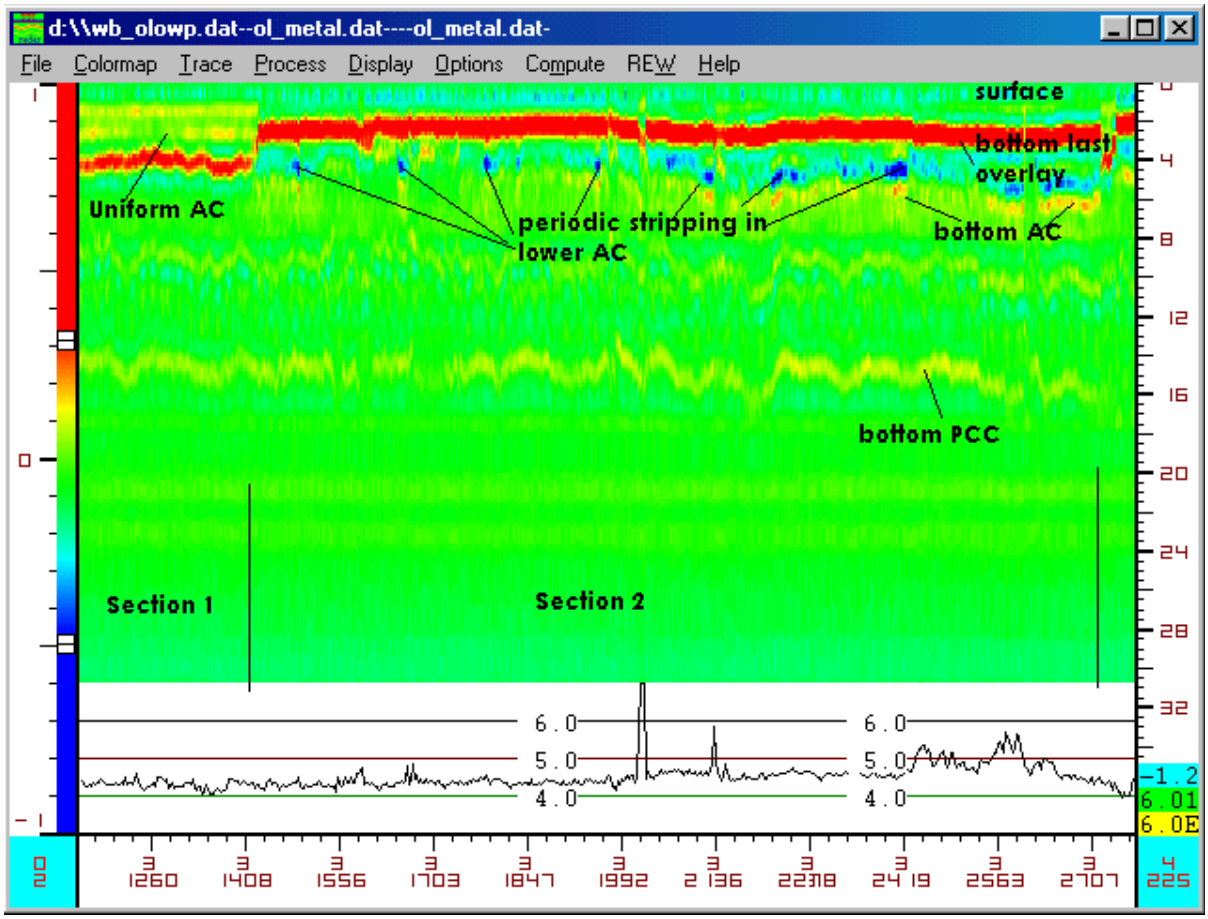

Figure 14. Potential Defect Areas on Westbound Outside Lane.

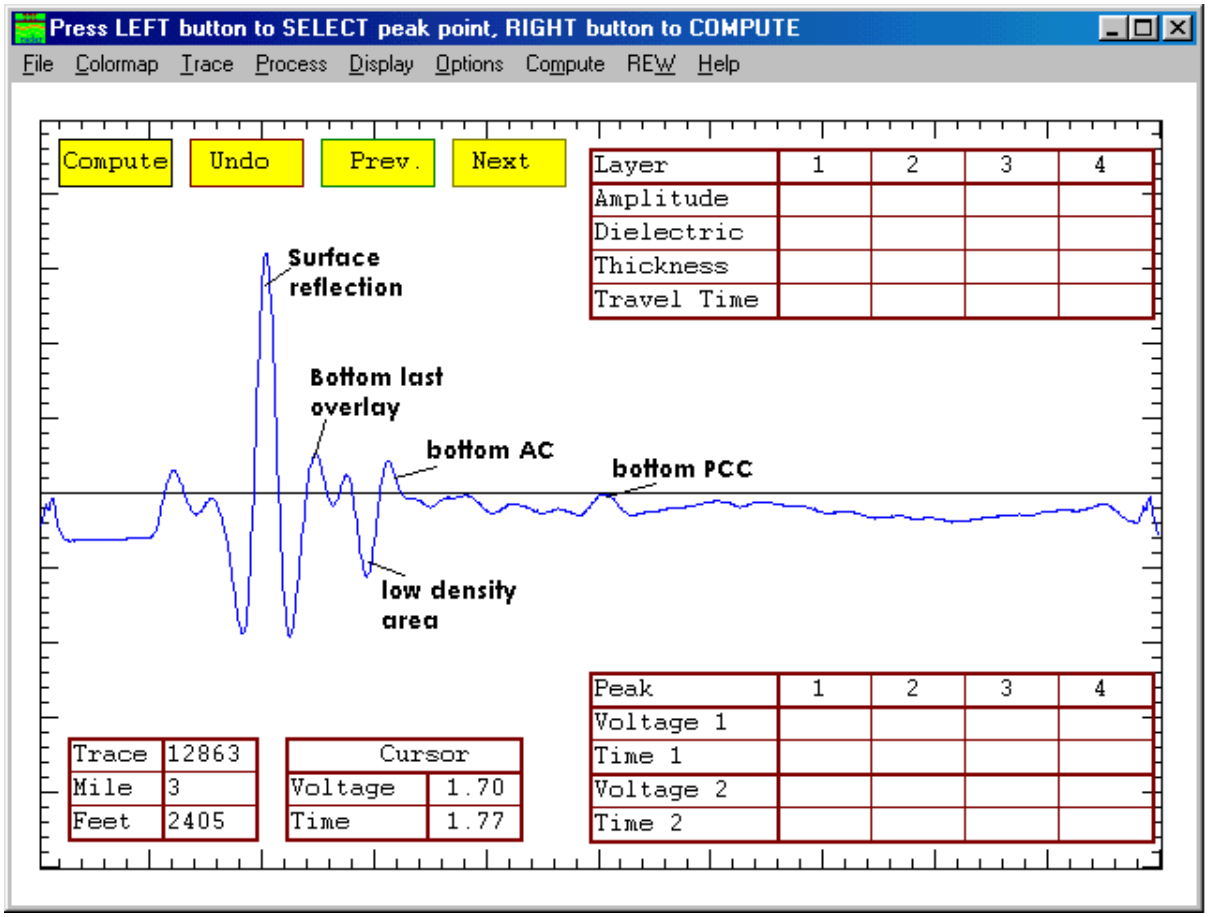

Figure 15. Individual Trace from an Area on the Westbound Outside Lane where Lower AC Layer Gives a Strong Negative Reflection.

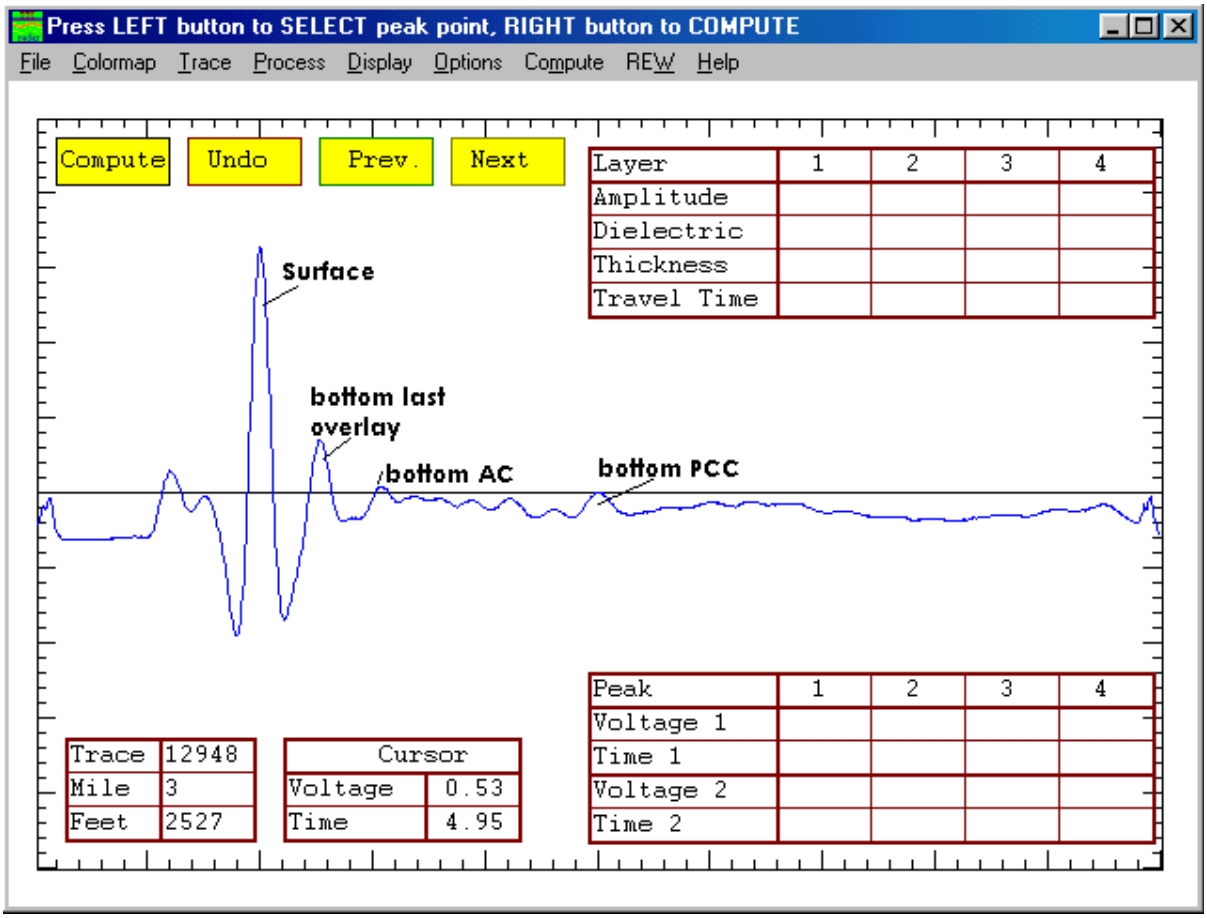

Figure 16. Individual Trace from a Normal Location on the Westbound Outside Lane.

Individual Traces from I-20 (Westbound)

Figures 15 and 16 show two individual traces from locations 100 feet apart in the westbound outside lane of I-20 (Figure 14). Figure 15 shows a strong negative reflection from the lower AC layer. The negative reflections are associated with the transition from a higher to a lower dielectric (density) area. In the past, this has been found to be associated with stripping in the lower AC layer.

Figure 16 is a trace from a normal area in the westbound direction. No defects are apparent at this location. The reflection from the top and bottom of the PCC are faint, but still clear in the data.

Summary

The GPR data, for the most part, show that the AC thickness on the project is fairly uniform. It is possible to see all of the major layer interfaces from the data. There are indications of potential stripping at various locations along the westbound outside lane that demonstrate the potential application of GPR for finding low density areas (such as at longitudinal joints or segregated areas) during construction of the experimental sections to be built along the I-20 overlay project.

CHAPTER III
WORK PLAN ESTABLISHED FOR CHARACTERIZING INITIAL PROPERTIES OF AS-BUILT TEST SECTIONS

This chapter simply documents the work plan for establishing a database of initial properties on the experimental test sections planned on the I-20 overlay project. The work plan was formulated by researchers in consultation with the TxDOT project director and program coordinator. The proposed tasks, which were planned for Phase II, were actually not conducted as the RMC decided to terminate Project 0-1708 at the end of the 2001 fiscal year.

TASK A. FIELD INVESTIGATIONS

This task has the following objectives:

- to establish sections for long-term performance monitoring which may be used to identify the effects of segregation, longitudinal joint density, ride quality, and construction uniformity on observed pavement performance;
- to collect field samples in randomly selected, potentially best, and potentially worst (defect) areas so that the engineering properties can be measured in the laboratory; and
- to rank the mixtures tested with respect to potential pavement performance based on the measured engineering properties.

Researchers will conduct field tests on the I-20 project in the Atlanta District. Nine test sections representing combinations of three different aggregates and three surface mixes are planned to be built. Researchers propose to monitor each section and conduct an extensive series of testing before, during, and after placement of the HMA surfacing layer. Field tests will include the activities listed in the following sections.

Pre-Overlay Testing

The I-20 project in the Atlanta District includes milling of the existing asphalt surface and repairs on the underlying continuously reinforced concrete (CRC) slab. Tests have

already been run on the existing pavement using GPR, SPA, FWD, and the Rolling Depth Deflectometer (RDD). After the CRC repairs are completed, Project 4185 researchers will run the SPA on the concrete slab to establish the variations of concrete modulus, slab thickness, and modulus of subgrade reaction along the project. In addition, Project 4185 researchers will obtain FWD as well as inertial profiler data to measure existing levels of roughness prior to placement of the overlay. TxDOT will collect RDD data. The data collected will serve the following purposes:

- to establish sections along the project for planning future pavement monitoring efforts by the Atlanta District,
- to provide information on the underlying layers to support future evaluations of pavement performance for assessing the cost-effectiveness of the different surface mixtures used in the project, and
- to evaluate the reduction in surface roughness after placement of the overlay.

Measurements and Testing During Placement of HMA (Quality Control Applications)

Researchers will use an infrared camera to measure the variation in surface temperature of the mat prior to compaction. The low temperature areas will be noted for future coring. Project 1708 researchers will collect material samples for laboratory testing to measure engineering properties of cracking potential, rut resistance, and permeability. Specific tests to be conducted are described later in this work plan. The reason for molding test specimens using asphalt mixtures sampled from the field and raw aggregates and binder is due to the difficulty in measuring material properties on cores taken from thin layers.

While the HMA is being placed, Project 4126 researchers will note the end of each load of HMA and denote locations where the paving operation stopped. At such locations, density profiles will be taken by Project 4126 researchers to identify segregated areas, if any. In addition, TxDOT will take cores and samples of the asphalt mixture for testing in the laboratory.

Measurements Taken Shortly After Compaction (Quality Assurance Applications)

The tools to be used here will be the portable SPA (PSPA) for measuring the modulus of the HMA layer, the GPR for measuring both thickness and density, the falling head

permeameter for measuring permeability on cores taken from the projects, and the inertial profiler for measuring overlay smoothness. With respect to the permeability measurements, there is currently no standard TxDOT test method for measuring the permeability of compacted asphalt concrete mixtures. Likewise, no standard test method has been established by the American Society for Testing and Materials (ASTM) nor by the American Association of State Highway and Transportation Officials. However, a test procedure was proposed by Izzo and Button (1997) in TxDOT Project 0-1238 which researchers will consider using in this project. Alternatively, Florida has a standard test method designated as Florida Method of Test FM 5-565 that uses the falling head permeameter shown in Figure 17 to determine the water conductivity of molded asphalt concrete specimens or cores. Researchers will decide which test procedure to use after consulting with the project director.

Areas to be tested will be the average and low mat temperature areas as identified by the infrared camera, locations where the paving operation stopped, and the longitudinal construction joints. Researchers will run the GPR along the wheel paths, middle of the lane, and near the construction joints, while PSPA data will be collected near the construction joints, at randomly selected areas where plant mix material has been sampled, and at potentially best and potentially worst areas identified from the infrared and density measurements. Longitudinal profile measurements will be made on both wheel paths of the final surface using TxDOT's inertial profiler.

Field Coring and Laboratory Testing

For this work, Projects 1708 and 4126 researchers will review the infrared, nuclear density, GPR, and PSPA measurements to identify potentially best and potentially worst (defect) areas in each of the nine test sections included in this rehabilitation project. Where these areas are identified, researchers propose to select one good and one defect area in each section where cores will be taken for laboratory characterizations of permeability, rut resistance, and cracking potential of the asphalt concrete mixtures. Researchers will coordinate with TxDOT's Atlanta District so that the cores can be taken within a reasonable time after the overlay is placed and the section is opened to traffic to minimize the influence of wheel loads and environmental factors on the laboratory measurements. From

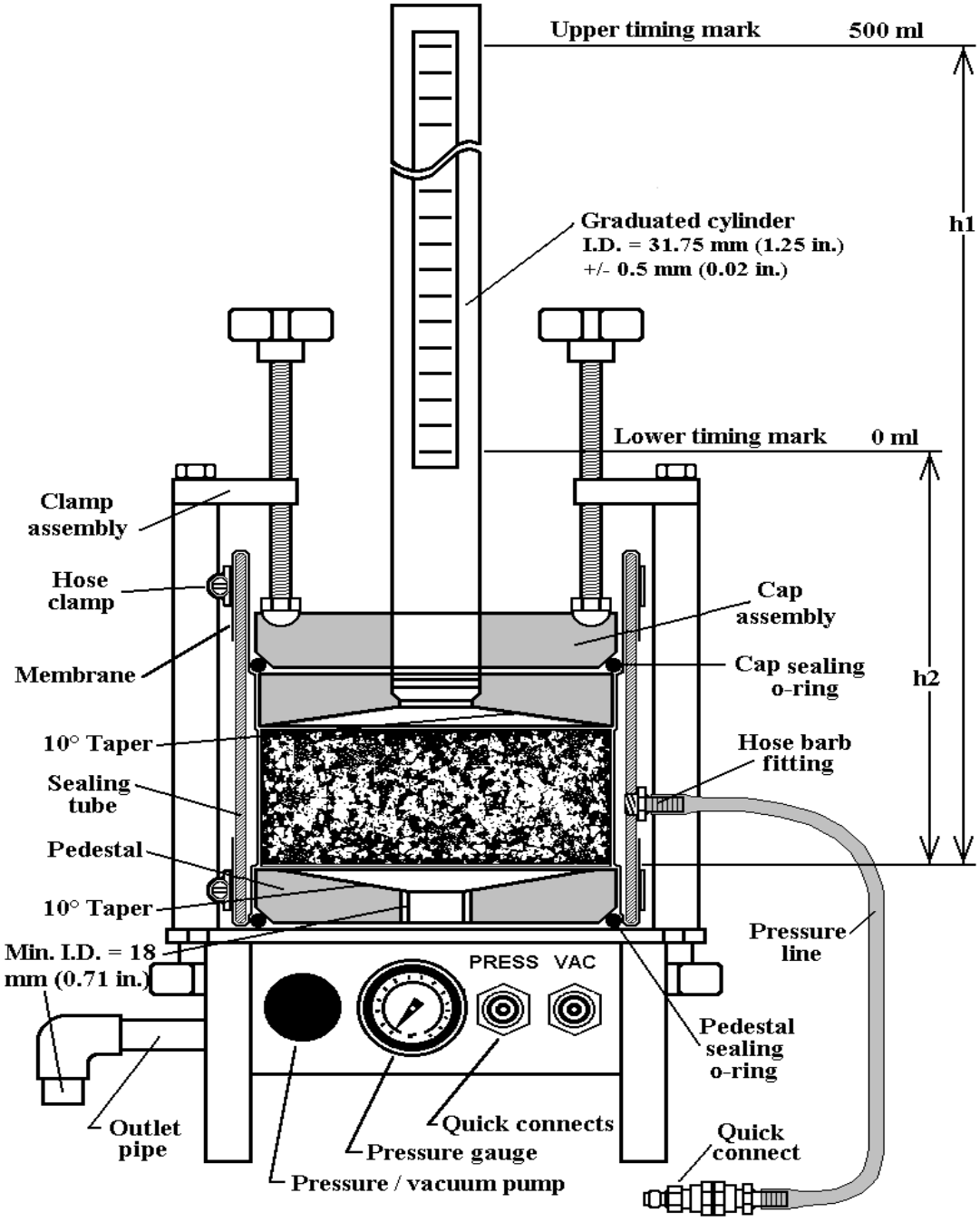

Figure 17. Florida Permeability Testing Apparatus.

conversations with TxDOT's Atlanta District laboratory engineer, the plan is to take cores within two weeks of placing the overlay on every two test sections.

Table 4 shows the tests that Project 1708 researchers plan to run on specimens of the surface mixtures. Researchers propose to run tests on cores considered to be representative of potentially best and potentially worst areas found in a given section (see Figure 18). In addition, cores will be taken at randomly selected areas where plant mix material has been sampled. Researchers will use this material to mold specimens for laboratory testing as shown in Table 4.

Cores and molded cylindrical specimens will be tested for permeability, rut resistance under the accelerated pavement analyzer (APA), and indirect tensile strength. Project 1708 researchers plan to determine the indirect tensile strength at room temperature and then use material from the broken specimen for extractions to obtain mixture proportions with which to calibrate the predictions from the PSPA and GPR. The APA tests will be conducted at a representative service temperature.

To evaluate cracking potential, Project 1708 researchers propose to cut slabs of the surface mix and prepare beam specimens for TTI's overlay tester. Assistance from TxDOT will be needed to remove the slabs. Figure 19 gives a schematic illustration of this test apparatus. In this test, the beam specimen is glued onto two platens, one of which is fixed and the other free to move parallel to the longitudinal axis of the specimen. It is then subjected to controlled displacement load cycles, with the crack growth monitored during the test. This information is used to rank reflection cracking resistance of the mixture tested. The plan is to conduct the overlay tests at one temperature (e.g., 20 °C) and two displacement levels, each with two replicates.

From a visual examination of the existing pavement at the site, transverse cracks extending the width of the travel lane were observed. Figure 20 shows a severe case where loose material has obviously been chipped off by road traffic. RDD data confirm that this crack development is due to reflection of the existing cracks in the underlying slab. For this reason, we propose to use the overlay tester to rank the reflection cracking resistance of the nine surface mixtures placed along the project.

Table 4. Proposed Laboratory Tests to Characterize As-Produced Engineering Properties.

Test	Number of Specimens		Nominal Dimensions (inches)	Comments
	Core/Beam[1]	Molded[2]		
Permeability	3	3	6(N) × 2(H)	FDOT FM 5-565
APA	3	3	6(N) × 2(H)	Use same specimens from permeability tests
Indirect Tensile Strength	2	2	4(N) × 2(H)	Test at room temperature to break cores for determining mixture proportions
Mixture Proportions	2	2	4(N) × 2(H)	Use for GPR and PSPA calibrations
Dynamic Modulus		4	4(N) × 8(H)	ASTM D3497
Permanent Deformation		4	4(N) × 8(H)	Use same specimens from dynamic modulus tests.
Overlay Tester	4	4	10(L) × 3(W) × 2(H)	

[1] For each randomly selected, potentially best and potentially worst area in a test section
[2] From plant mix corresponding to randomly selected area in a test section

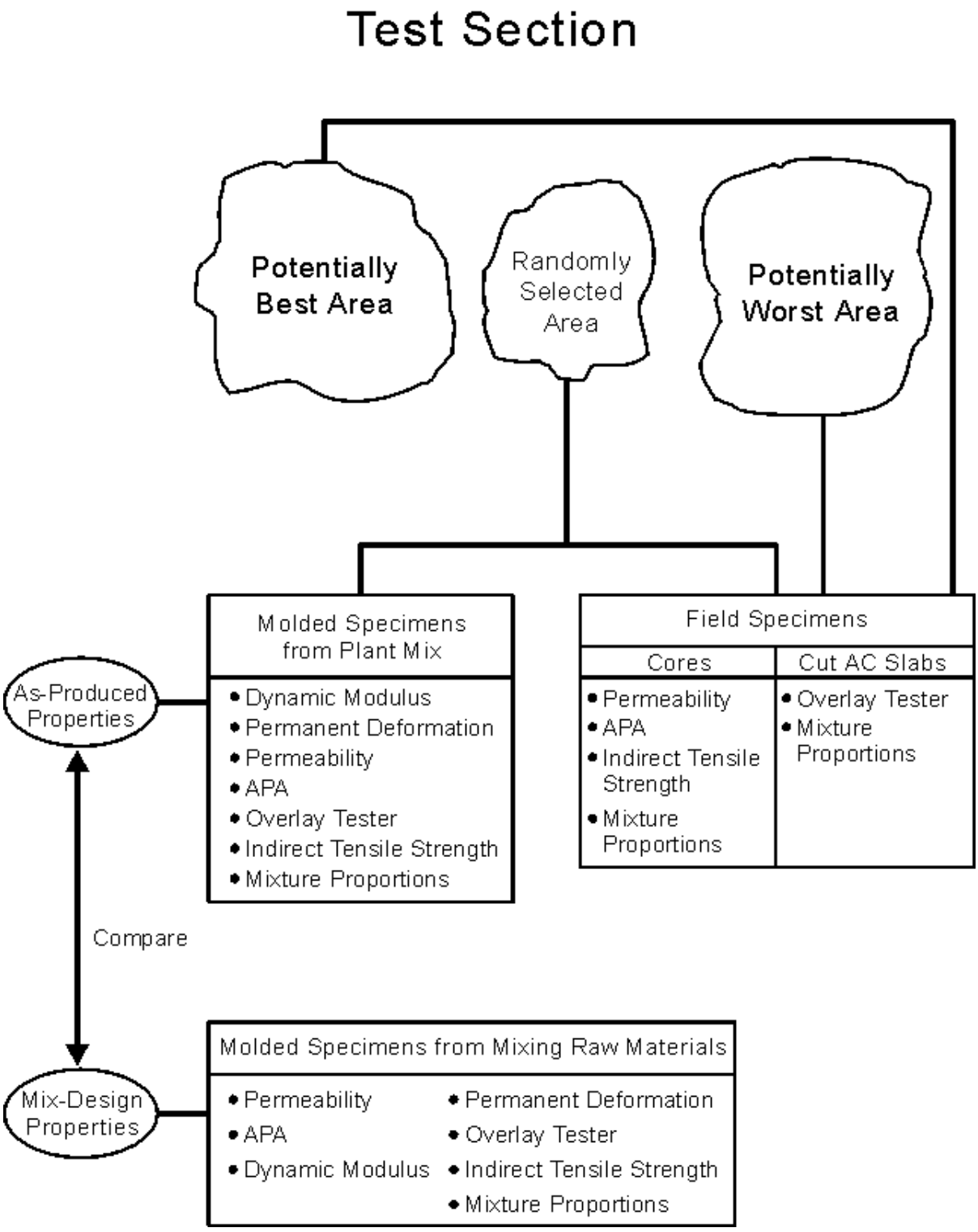

Figure 18. Laboratory Tests Planned for Each Test Section on the I-20 Overlay Project.

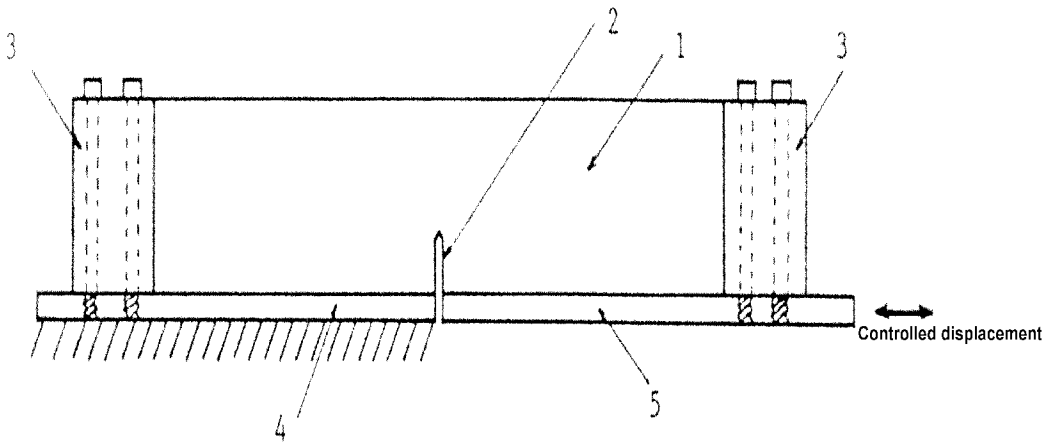

Figure 19. Schematic Illustration of Overlay Tester.

Figure 20. Photo of Severe Transverse Cracking along the I-20 Project.

For dynamic modulus testing, it will not be possible to test cores as the thickness will not meet the size requirements specified in ASTM D3497. Researchers therefore propose to take samples of the plant mix and mold 4-inch diameter by 8-inch high specimens corresponding to the measured field density at the randomly selected area where the material has been sampled. For specimen preparation, the Superpave press will be used to mold specimens of the different mixtures. For any given specimen, researchers will first characterize the dynamic modulus and then the permanent deformation. For the latter, the increase in permanent deformation with repeated loading will be monitored to characterize the permanent deformation properties of a given mix. Researchers plan to run permanent deformation tests at two temperatures, each with two replicates. Figure 21 illustrates test data from repeated load permanent deformation tests.

To provide a reference for comparing the different surface mixtures in terms of their engineering properties, researchers also plan to mold specimens in the laboratory by blending samples of the raw materials (asphalt and aggregates) according to the design of the given mix. This is shown in Figure 18. Researchers will then run the battery of tests listed in Table 4 to characterize the engineering properties of the molded specimens and establish reference values with which to evaluate the quality of the in-place mixtures in Task C.

TASK B. COMPILE DATA ON MEASURED PROPERTIES

In this task, Project 1708 researchers will compile the data from Task A into electronic files that characterize the initial, as-built state of the sections tested. Table 5 shows the data to be collected on the I-20 overlay project in the Atlanta District. The following data will be collected in this research project:

- mixture proportions - asphalt type and source; aggregate type, source and gradation; air voids content; asphalt content; and voids in mineral aggregate (VMA);
- engineering properties - rut resistance as evaluated from APA and permanent deformation tests, cracking resistance from overlay tester and indirect tensile test, dynamic modulus, and permeability;

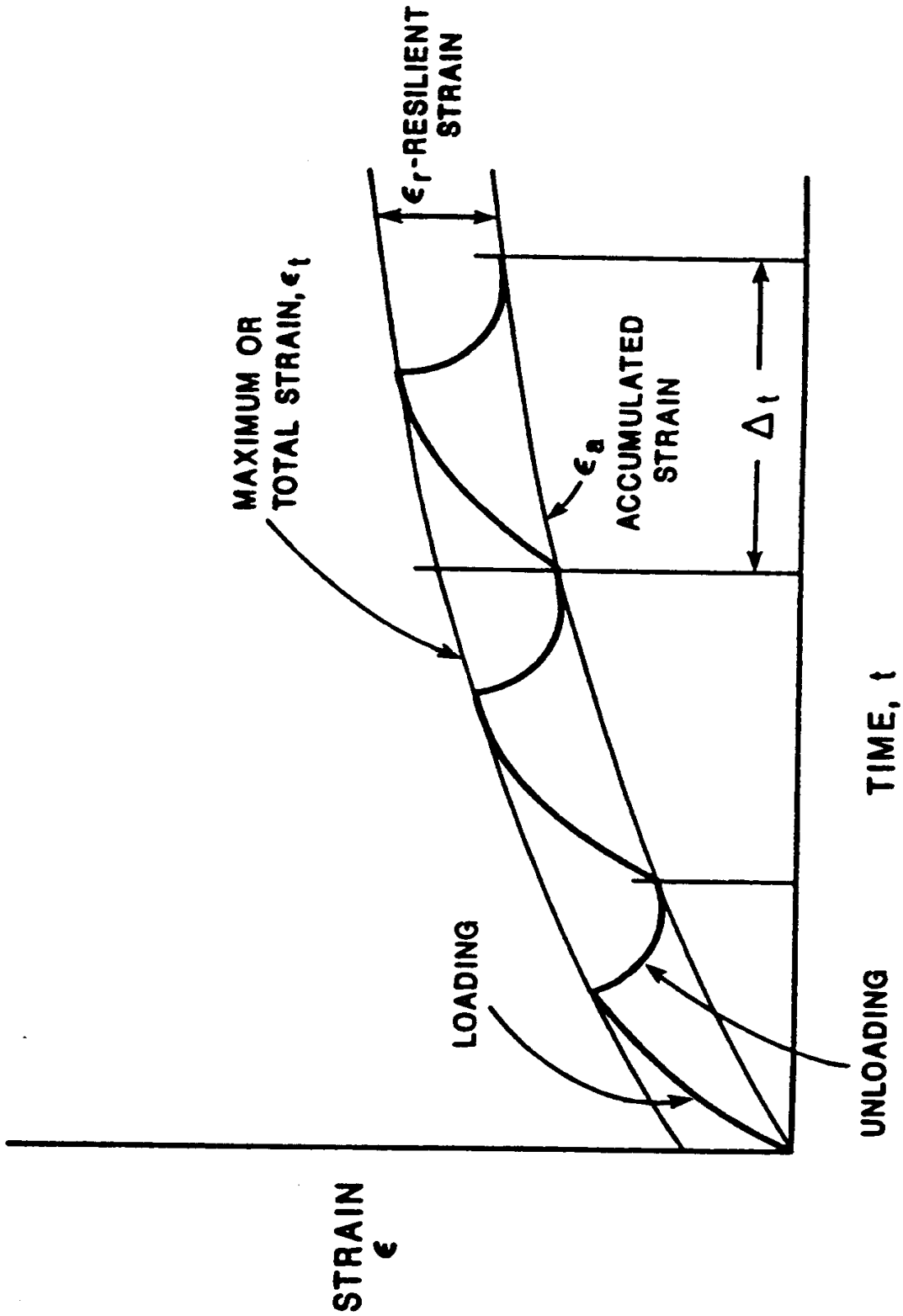

Figure 21. Conceptual Illustration of Data from Permanent Deformation Test.

Table 5. Data to be Collected on I-20 Overlay Project in the Atlanta District.

Data	Laboratory Tests					Construction-Related Tests			Pavement Condition Monitoring
	Molded Specimens		AC Cores/Beams			Existing Pavement	After CRCP Repairs	Overlay	
	Mix Design	As-Produced (plant mix)	Random Sample	Potentially Best	Potentially Worst				
Tests for Engineering Properties (Potential Performance Indicators)									
•Permeability	✓	✓	✓	✓	✓				
•APA	✓	✓	✓	✓	✓				
•Permanent deformation	✓	✓							
•Overlay tester	✓	✓	✓	✓	✓				
•Dynamic modulus	✓	✓							
•Indirect tensile strength	✓	✓	✓	✓	✓				
•Hamburg (Project 4185)	✓	✓	✓						
•Moisture sensitivity - 531C (TxDOT)	✓								
•Binder properties from DSR (TxDOT)	✓	✓	✓	✓	✓				
Mixture Proportions									
•Binder content	✓	✓	✓	✓	✓				
•Air voids (from molded specimen/core)	✓	✓	✓	✓	✓				
•Air voids (from remolded core)			✓	✓	✓				
•Gradation	✓	✓	✓	✓	✓				
Nondestructive tests									
•GPR[1] (Project 4185)						✓		✓	✓
•SPA (Project 4185)						✓	✓	✓	✓
•PSPA								✓	
•Infrared (Project 4126)								✓	
•Nuclear density gauge (Project 4126)								✓	
•Pavetracker[2]								✓	
•FWD (Project 4185)						✓	✓	✓	✓
•RDD (TxDOT)						✓	✓	✓	✓
Pavement Performance Indicators									
•Ride quality (Project 4185)						✓	✓	✓	✓
•Distress (Project 4185)							✓	✓	✓
•Traffic - WIM data (TxDOT)								✓	✓

[1] GPR to provide thickness and density profiles

[2] New device for measuring density

- Quality Control (QC)/Quality Assurance (QA) test data - initial surface smoothness; longitudinal joint density measurements from GPR; and segregated areas as identified from nuclear density gauge, cores, GPR, and PSPA; and
- pavement structure information - variation in overlay thickness from GPR and variations in CRC slab modulus, slab thickness, and modulus of subgrade reaction from PSPA.

In addition to the above, Table 5 shows tests to be conducted by TxDOT on Project 0-4185 that will provide additional data for future evaluation of the relationships between construction quality indicators and pavement performance. Project 1708 researchers will coordinate with Project 4185 and Project 4126 research staff to ensure no duplication of work.

Field verification of the impact of construction quality on pavement performance will require a long-term monitoring program on the Atlanta project. Whether this program will be conducted in-house by TxDOT or through an interagency agreement is a decision TxDOT will have to make after this research project. Long-term pavement performance monitoring will require periodic visual distress surveys, nondestructive tests, and characterization of the truck axle loadings using the weigh-in-motion (WIM) pads to be installed by TxDOT at the site.

TASK C. EVALUATE IMPACT OF CONSTRUCTION QUALITY

Project 1708 researchers will assess the impact of construction quality by comparing measured engineering properties corresponding to as-built conditions with engineering properties corresponding to the mix design. Our plan is to simply rank the mixtures tested in terms of:

- rut resistance as evaluated from the APA, permanent deformation, and dynamic modulus tests;
- cracking resistance as evaluated from the overlay tester and indirect tensile strength tests; and
- propensity to moisture-related damage based on the permeability tests and Hamburg test findings from Project 0-4185.

In this way, the impact of construction quality will be evaluated in terms of the effects on engineering properties which are known to correlate to pavement performance.

For each of the three criteria given above, the related engineering properties will be compiled into a test matrix (Table 6). Project 1708 researchers will then compare the different cells in the matrix to group the mixtures tested according to potential performance based on the given criterion. The results may be used to identify engineering properties and establish desirable levels of these properties for QC/QA specifications. Where significant differences in engineering properties are found, the mixture proportions will be investigated to determine if the differences in engineering properties can be explained by variations in basic mixture properties such as binder content, air voids content, and gradation. Researchers recommend a monitoring program after the project is completed to verify the correlations between the rankings determined in this task, engineering properties from the tests conducted, and actual pavement performance of the sections built.

TASK D. PHASE II REPORT

At the end of Phase II, a research report will be prepared that:

- documents the tests conducted in Task A to characterize the as-built properties of the Atlanta test sections and the target properties from the mix designs;
- presents the results of the comparative analysis in Task C to group the mixtures in terms of rutting resistance, cracking resistance, and propensity to moisture-related damage using the engineering properties determined in Task A; and
- summarizes the findings with respect to engineering properties and desirable levels of these properties to achieve good performing mixtures.

Additionally, the test data compiled in Task B will be provided in electronic files at the end of the research project.

Table 6. Matrix of Test Results for Comparing Mixtures Tested.

Construction Quality Level	Aggregate Type	Surface Mix		
		CMHB[1]-C	Type C	½" Superpave
Potentially Best	Quartzite			
	Sandstone			
	Siliceous River Gravel			
Potentially Worst	Quartzite			
	Sandstone			
	Siliceous River Gravel			
Random Sample	Quartzite			
	Sandstone			
	Siliceous River Gravel			
Mix Design	Quartzite			
	Sandstone			
	Siliceous River Gravel			

[1] Coarse matrix high binder

REFERENCES

Aouad, M. F., Stokoe II, K. H., and Briggs, R. C. (1993), "Stiffness of Asphalt Concrete Surface Layer from Stress Wave Measurements," Transportation Research Record 1384, Washington, D.C., pp. 29-35.

Dobry, R., and Gazetas, G. (1986), "Dynamic Response of Arbitrary Shaped Foundations," *Journal of Geotechnical Engineering* (American Society of Civil Engineers, New York) 112, no. 2, 2:109-35.

Fernando, E., Prabhakar, V., Scullion, T., and Nazarian, S. (2000), "Predicting Hot-Mix Performance from Measured Properties: Phase I Report," Research Report 1708-1, Texas Transportation Institute, Texas A&M University, College Station, TX.

Izzo, R. P., and Button, J. (1997), "Permeability of Coarse Matrix-High Binder Mixtures and Its Effects on Performance," Research Report 1238-1F, Texas Transportation Institute, Texas A&M University, College Station, TX.

Li, Y., and Nazarian, S. (1994), "Evaluation of Aging of Hot-Mix Asphalt Using Wave Propagation Techniques," STP 1265, American Society for Testing and Materials, Philadelphia, PA, pp. 166-179.

McDaniel, M., Yuan, D., Chen, D. H., and Nazarian, S. (1999), "Use of Seismic Pavement Analyzer in Forensic Studies in Texas," STP 1735, ASTM, West Conshohocken, PA.

National Cooperative Highway Research Project (1996), "Nondestructive Testing to Determine Material Properties of Pavement Layers," Interim Report, NCHRP 10-44, Washington, D.C.

Nazarian, S., and Bush, A. (1990), "Determination of Surface Deflection of Pavement Systems Using Velocity Transducers," Transportation Research Record 1227, Washington, D.C., pp. 147-158.

Nazarian, S., Reddy, S., and Baker, M. R. (1994), "Determination of Voids Under Rigid Pavements Using Impulse Response Method," STP 1198, ASTM, Philadelphia, PA, pp. 473-487.

Nazarian, S., Baker, M., and Crain, K. (1997), "Assessing Quality of Concrete with Wave Propagation Techniques," Materials Journal, American Concrete Institute, Vol. 94, No. 4, Farmington Hills, MI, pp. 296-306.

Reddy, S. (1992), "Determination of Voids in Rigid Pavements Using the Impulse Response Method," M.S. thesis, The University of Texas at El Paso, El Paso, TX.

Saarenketo, T. (1996), "Using GPR and Dielectric Probe Measurements in Pavement Density Quality Control," Transportation Research Record 1997, Transportation Research Board, Washington, D.C., pp. 34-41.

Saarenketo, T., and Scullion, T. (1995), "Using Electrical Properties to Classify the Strength Properties of Base Course Aggregates," Research Report 1341-2, Texas Transportation Institute, Texas A&M University, College Station, TX.

Sansalone, M., and Carino, N. J. (1986), "Impact-Echo: A Method for Flaw Detection in Concrete Using Transient Stress Waves," Report NBSIR 86-3452. National Bureau of Standards, Gaithersburg, MD.

Scullion, T., and Chen, Y. (1999), "COLORMAP Version 2 User's Guide with Help Menus," Research Report 1702-4, Texas Transportation Institute, Texas A&M University, College Station, TX.

APPENDIX A
SEISMIC MODULI PREDICTED FROM SPA TESTING

Table A1. Seismic Moduli Predicted from SPA Tests along Eastbound Left Lane.

Station	AC Temp. (°F)	Phase Velocity from USW, m/sec		Velocity Ratio	AC Modulus (ksi)	IR Modulus (ksi)
		from A32	from A43			
1135+00	95	1423	2119	1.49	727	197
1136+01	95	1554	1993	1.28	867	147
1135+02	95	1489	1517	1.02	796	111
1135+03	95	1617	1400	0.87	938	173
1135+04	96	1425	1520	1.07	735	174
1140+00	96	1475	1455	0.99	788	180
1140+01	96	1615	1462	0.91	945	154
1140+02	96	1408	1579	1.12	718	276
1140+03	96	1592	1630	1.02	918	147
1140+04	97	1574	1081	0.69	906	219
1140+05	97	1678	1300	0.77	1029	99
1140+06	97	1614	1514	0.94	952	151
1150+01	97	1445	1371	0.95	763	95
1150+02	97	1365	1399	1.02	681	151
1150+03	97	1440	1351	0.94	758	216
1150+04	98	1254	1156	0.92	580	104
1150+05	98	1179	1112	0.94	513	196
1150+06	98	1583	1276	0.81	924	166
1150+07	98	1478	1331	0.90	806	120
1150+08	98	1459	1480	1.01	785	101
1150+09	99	1589	1593	1.00	940	128
1160+00	99	1589	1056	0.66	940	125
1160+01	100	1453	1525	1.05	794	149
1160+02	100	1413	1356	0.96	751	104
1160+03	100	1446	1543	1.07	786	112
1160+04	100	1422	1033	0.73	760	126
1160+05	100	1629	1546	0.95	998	108
1160+06	101	1511	1957	1.30	866	114
1160+07	101	1437	1162	0.81	784	111
1160+08	101	1393	1034	0.74	736	112
1160+09	101	1444	1351	0.94	791	124
1170+00	101	1526	1289	0.84	884	26
1170+01	102	1258	1502	1.19	606	164
1170+02	102	1554	1801	1.16	925	171
1170+03	102	1484	1030	0.69	844	211
1170+04	102	1297	1382	1.07	645	111
1180+00	102	1622	1879	1.16	1008	179
1180+01	103	1378	1615	1.17	735	271
1180+02	103	1482	1561	1.05	850	203
1180+03	103	1352	1666	1.23	707	183
1180+04	103	1142	1445	1.27	505	160
1180+05	103	1523	1200	0.79	897	147
1180+06	104	1525	1186	0.78	909	239
1180+07	104	1348	1325	0.98	710	144
1180+08	104	1286	1407	1.09	646	89

Table A1. Seismic Moduli Predicted from SPA Tests along Eastbound Left Lane (continued).

Station	AC Temp. (°F)	Phase Velocity from USW, m/sec		Velocity Ratio	AC Modulus (ksi)	IR Modulus (ksi)
		from A32	from A43			
1180+09	104	1512	1309	0.87	893	149
1190+00	103	1444	992	0.69	807	240
1190+01	103	1458	1467	1.01	822	137
1190+02	103	1610	1172	0.73	1003	92
1190+03	103	1396	1376	0.99	754	140
1190+04	102	1507	1158	0.77	870	143
1190+05	102	1233	1346	1.09	583	164
1190+06	102	1523	1056	0.69	889	81
1190+07	102	1505	1652	1.10	868	84
1190+08	101	1544	1705	1.10	905	193
1190+09	101	1633	1357	0.83	1012	93
1200+00	101	1455	1669	1.15	803	67
1200+01	101	1308	1338	1.02	649	94
1200+02	100	1556	1239	0.80	910	179
1200+03	100	1401	1301	0.93	738	96
1200+04	100	1583	1017	0.64	942	159
1200+05	100	1183	1776	1.50	526	115
1200+06	99	1383	1364	0.99	712	303
1200+07	99	1454	1029	0.71	787	128
1200+08	99	1557	1590	1.02	903	117
1200+09	99	1428	1251	0.88	759	184
1210+00	98	1469	1528	1.04	796	221
1210+01	98	1530	1490	0.97	864	196
1210+02	98	1399	1564	1.12	722	116
1210+03	98	1626	1583	0.97	975	121
1210+04	97	1269	1769	1.39	589	167
1210+05	97	1571	1397	0.89	902	127
1210+06	97	1491	1638	1.10	813	181
1210+07	97	1573	1270	0.81	904	159
1210+08	96	1538	1656	1.08	857	173
1210+09	96	1453	1481	1.02	765	82
1220+00	96	1447	861	0.60	758	166
1220+01	96	1405	1419	1.01	715	131
1220+02	95	1536	1423	0.93	847	183
1220+03	95	1478	1447	0.98	784	247
1220+04	95	1576	1553	0.99	891	78
1220+05	95	1326	1494	1.13	631	104
1220+06	95	1486	1573	1.06	793	234
1220+07	94	1334	1348	1.01	633	118
1220+08	94	1382	1316	0.95	679	117
1220+09	94	1553	1137	0.73	858	153
1230+00	94	1532	1948	1.27	835	189
1230+01	94	1365	998	0.73	663	139
1230+02	93	1327	1609	1.21	621	139

Table A1. Seismic Moduli Predicted from SPA Tests along Eastbound Left Lane (continued).

Station	AC Temp. (°F)	Phase Velocity from USW, m/sec		Velocity Ratio	AC Modulus (ksi)	IR Modulus (ksi)
		from A32	from A43			
1230+03	93	1311	1040	0.79	606	177
1230+04	93	1553	1646	1.06	850	173
1230+05	93	1587	1398	0.88	888	137
1230+06	93	1539	1048	0.68	835	186
1230+07	93	1515	1424	0.94	809	190
1230+08	93	1713	1423	0.83	1034	159
1230+09	93	1557	1668	1.07	855	186
1240+00	92	1350	1667	1.23	637	134
1240+01	92	1598	1545	0.97	892	166
1240+02	92	1602	1686	1.05	897	177
1246+00	92	1620	1448	0.89	917	141
1247+00	92	1426	1565	1.10	711	237
1240+08	92	1536	1642	1.07	824	153
1240+09	92	1579	1660	1.05	871	116
1250+00	92	1560	1547	0.99	850	36
1250+01	91	1276	1355	1.06	564	
1250+02	91	1701	1037	0.61	1002	236
1250+03	91	1561	1661	1.06	844	123
1250+04	91	1617	945	0.58	906	105
1250+05	91	1496	1367	0.91	775	146
1250+06	91	1390	1424	1.02	669	179
1250+07	91	1503	1603	1.07	782	164
1250+08	91	1684	1492	0.89	982	239
1250+09	91	1459	1499	1.03	737	153
1260+00	91	1557	1670	1.07	840	211
1260+01	91	1517	1568	1.03	797	289
1260+02	91	1635	1929	1.18	926	27
1260+03	90	1584	1288	0.81	862	206
1260+04	90	1569	1061	0.68	845	191
1260+05	90	1446	1551	1.07	718	199
1260+06	89	1356	984	0.73	626	140
1260+07	89	1464	1205	0.82	730	25
1260+08	89	1562	1192	0.76	831	161
1260+09	88	1525	1748	1.15	785	20
1270+00	88	1471	1402	0.95	730	147
1270+01	88	1690	1162	0.69	964	126
1270+02	88	1555	1352	0.87	816	173
1270+03	88	1458	1657	1.14	718	210
1270+04	88	1534	1428	0.93	794	154
1270+05	88	1614	1566	0.97	879	160
1270+06	88	1206	1834	1.52	491	159
1270+07	88	1203	1777	1.48	488	193
1270+08	88	1614	1891	1.17	879	206
1270+09	88	1687	1395	0.83	961	141

Table A1. Seismic Moduli Predicted from SPA Tests along Eastbound Left Lane (continued).

Station	AC Temp. (°F)	Phase Velocity from USW, m/sec		Velocity Ratio	AC Modulus (ksi)	IR Modulus (ksi)
		from A32	from A43			
1280+00	88	1469	940	0.64	728	163
1280+01	88	1533	1448	0.94	793	189
1280+02	88	1567	1424	0.91	829	140
1280+03	88	1295	1541	1.19	566	151
1280+04	88	1468	1265	0.86	727	122
1280+05	88	1592	1470	0.92	855	16
1280+06	88	1629	1166	0.72	896	166
1280+07	88	1599	1182	0.74	863	213
1280+08	88	1459	1741	1.19	719	131
1280+09	88	1355	1534	1.13	620	231
1290+00	88	1519	1308	0.86	779	124
1290+01	87	1208	2069	1.71	488	293
1290+02	87	1561	1346	0.86	816	167
1290+03	87	1408	1448	1.03	664	243
1290+04	87	1511	1648	1.09	764	181
1290+05	87	1606	1480	0.92	863	167
1290+06	87	1513	1703	1.13	766	106
1290+07	87	1358	1840	1.35	617	147
1290+08	87	1165	1457	1.25	454	253
1290+09	87	1498	1446	0.97	751	234
1300+00	87	1609	1520	0.94	866	113
1300+01	86	1607	1351	0.84	857	219
1300+02	86	1470	1329	0.90	717	110
1300+03	86	1559	1307	0.84	807	187
1300+04	86	1410	1476	1.05	660	107
1300+05	86	1571	1585	1.01	819	154
1300+06	86	1576	1175	0.75	824	221
1300+07	86	1523	971	0.64	770	166
1300+08	86	1453	1124	0.77	701	263
1300+09	86	1249	2086	1.67	518	131
1310+00	86	1230	1517	1.23	502	92
1310+01	86	1502	1529	1.02	749	171
1310+03	86	1461	2271	1.55	708	344
1310+04	86	1535	1586	1.03	782	236
1310+05	86	1567	963	0.61	815	309
1310+06	86	1524	1012	0.66	771	231
1310+07	86	1518	1522	1.00	765	107
1310+08	85	1618	1628	1.01	862	15
1310+09	85	1532	1442	0.94	773	244
1320+00	85	1624	1025	0.63	868	260
1320+01	85	1266	1101	0.87	528	119

Table A2. Seismic Moduli Predicted from SPA Tests along Eastbound Right Lane.

Station	AC Temp. (°F)	Phase Velocity from USW, m/sec		Velocity Ratio	AC Modulus (ksi)	IR Modulus (ksi)
		from A32	from A43			
1135+00	74	1785	2097	1.17	961	201
1136+01	74	1738	1773	1.02	911	40
1135+02	74	1728	1169	0.68	901	130
1135+03	74	1811	1897	1.05	989	53
1135+04	74	1700	1921	1.13	872	156
1140+00	74	1832	1499	0.82	1012	84
1140+01	74	1781	1870	1.05	957	159
1140+02	74	1782	1816	1.02	958	104
1140+03	74	1904	1064	0.56	1093	55
1140+04	74	1832	1810	0.99	1012	21
1140+05	74	1627	1723	1.06	798	21
1140+06	74	1680	993	0.59	851	25
1150+01	74	1409	1201	0.85	599	154
1150+02	74	1686	1753	1.04	857	239
1150+03	74	1810	1833	1.01	988	129
1150+04	74	1745	1843	1.06	918	119
1150+05	74	1849	1806	0.98	1031	102
1150+06	74	1790	1930	1.08	966	99
1150+07	74	1867	1848	0.99	1051	102
1150+08	74	1852	1817	0.98	1035	154
1150+09	74	1890	1895	1.00	1077	131
1160+00	74	1825	1780	0.98	1005	206
1160+00	74	1833	1784	0.97	1013	131
1160+01	74	1729	1871	1.08	902	176
1160+02	74	1354	1514	1.12	553	111
1160+03	74	1682	1859	1.11	853	79
1160+04	74	1644	1790	1.09	815	67
1160+05	74	1701	1808	1.06	873	25
1160+06	74	1668	1821	1.09	839	24
1160+07	74	1724	1916	1.11	896	159
1160+08	74	1703	1807	1.06	875	119
1160+09	74	1748	1666	0.95	922	132
1170+00	74	1493	1875	1.26	672	160
1170+01	74	1612	1565	0.97	784	263
1170+02	74	1440	1102	0.77	625	164
1170+03	74	1615	1660	1.03	787	166
1170+04	74	1321	1073	0.81	526	200
1180+00	74	1443	1627	1.13	628	200
1180+01	74	1346	1634	1.21	546	237
1180+02	74	1479	1113	0.75	660	151
1180+02	74	1407	1825	1.30	597	237
1180+03	74	1454	1482	1.02	638	176
1180+04	74	1554	2107	1.36	728	174
1180+05	74	1612	1687	1.05	784	189
1180+06	75	1326	1152	0.87	534	144
1180+07	75	1671	1741	1.04	849	190

Table A2. Seismic Moduli Predicted from SPA Tests along Eastbound Right Lane (continued).

Station	AC Temp. (°F)	Phase Velocity from USW, m/sec		Velocity Ratio	AC Modulus (ksi)	IR Modulus (ksi)
		from A32	from A43			
1180+08	75	1590	1834	1.15	768	140
1180+09	75	1587	1772	1.12	765	109
1190+00	75	1675	1885	1.13	853	134
1190+00	75	1659	1886	1.14	837	110
1190+01	75	1648	1675	1.02	825	20
1190+02	76	1635	1788	1.09	819	201
1190+03	76	1619	1740	1.07	803	177
1190+04	76	1723	1853	1.08	909	144
1190+05	76	1626	1756	1.08	810	174
1190+06	76	1662	1682	1.01	846	140
1190+07	76	1666	1726	1.04	850	151
1190+08	76	1635	957	0.59	819	149
1190+09	77	1622	1676	1.03	812	134
1200+00	77	1532	1515	0.99	724	24
1200+00	77	1554	1505	0.97	745	139
1200+00	77	1556	1505	0.97	747	83
1200+01	77	1815	1161	0.64	1017	32
1200+02	77	1714	1587	0.93	907	121
1200+03	77	1750	1448	0.83	945	333
1200+04	77	1640	1268	0.77	830	18
1200+05	78	1657	1100	0.66	854	27
1200+06	78	1788	1486	0.83	995	170
1200+07	78	1839	1727	0.94	1052	150
1200+08	78	1800	1763	0.98	1008	180
1210+00	78	1761	1265	0.72	965	136
1210+00	78	1765	1268	0.72	969	121
1210+01	78	1752	1153	0.66	955	137
1210+02	78	1616	1314	0.81	812	144
1210+03	78	1549	1373	0.89	746	231
1210+04	78	1720	1444	0.84	920	117
1210+05	78	1652	1558	0.94	849	169
1210+06	78	1870	1270	0.68	1088	170
1210+07	78	1901	1374	0.72	1124	143
1210+08	78	1871	1644	0.88	1089	116
1210+09	78	1776	1634	0.92	981	43
1220+00	78	1766	1694	0.96	970	66
1220+00	78	1753	1708	0.97	956	207
1220+01	78	1523	977	0.64	722	49
1220+02	78	1796	1297	0.72	1003	247
1220+03	78	1709	1328	0.78	909	210
1220+04	78	1687	1740	1.03	885	52
1220+05	78	1556	1073	0.69	753	209
1220+06	78	1763	1291	0.73	967	19
1220+07	78	1775	1213	0.68	980	17

Table A2. Seismic Moduli Predicted from SPA Tests along Eastbound Right Lane (continued).

Station	AC Temp. (°F)	Phase Velocity from USW, m/sec		Velocity Ratio	AC Modulus (ksi)	IR Modulus (ksi)
		from A32	from A43			
1220+08	78	1803	1256	0.70	1011	
1220+09	78	1821	1620	0.89	1032	244
1230+00	78	1620	1455	0.90	816	20
1230+01	78	1688	1809	1.07	886	90
1230+00	79	1728	1851	1.07	936	55
1230+02	79	1745	1128	0.65	955	141
1230+03	79	1907	1227	0.64	1140	17
1230+04	79	1488	1094	0.74	694	16
1230+05	80	1627	1268	0.78	837	16
1230+06	80	1712	1246	0.73	926	150
1230+07	80	1636	1689	1.03	846	123
1230+08	80	1292	1201	0.93	528	227
1230+09	80	1722	1342	0.78	937	110
1240+00	81	1660	1196	0.72	878	93
1240+00	81	1745	1182	0.68	970	21
1240+01	81	1629	1136	0.70	845	94
1240+02	81	1755	1029	0.59	981	153
1246+00	81	1681	1177	0.70	900	126
1247+00	81	1473	1218	0.83	691	110
1240+08	81	1723	1462	0.85	946	113
1240+09	81	1440	1390	0.97	661	72
1250+00	81	1712	1474	0.86	934	42
1250+00	81	1746	1476	0.85	971	
1250+01	81	1629	1390	0.85	845	72
1250+02	81	1524	1407	0.92	740	169
1250+03	81	1660	1734	1.04	878	88
1250+04	81	1632	1199	0.73	849	
1250+05	81	1877	1322	0.70	1122	193
1250+06	81	1615	1174	0.73	831	
1250+07	81	1777	1120	0.63	1006	83
1250+08	81	1704	1435	0.84	925	244
1250+09	81	1714	1714	1.00	936	
1260+00	81	1688	1205	0.71	908	
1260+00	81	1656	1200	0.72	874	236
1260+01	82	1683	1170	0.70	910	108
1260+02	82	1489	1558	1.05	712	105
1260+03	82	1559	1978	1.27	781	58
1260+03	82	1595	1983	1.24	817	21
1260+04	83	1552	1182	0.76	780	135
1260+05	83	1670	1143	0.68	903	134
1260+06	83	1650	1093	0.66	881	51
1260+07	83	1682	1791	1.06	916	147
1260+08	83	1577	1589	1.01	805	92
1260+09	83	1748	1280	0.73	989	82

Table A2. Seismic Moduli Predicted from SPA Tests along Eastbound Right Lane (continued).

Station	AC Temp. (°F)	Phase Velocity from USW, m/sec		Velocity Ratio	AC Modulus (ksi)	IR Modulus (ksi)
		from A32	from A43			
1270+00	84	1616	1732	1.07	852	280
1270+00	84	1677	1795	1.07	918	119
1270+01	84	1621	1423	0.88	858	174
1270+02	84	1616	1756	1.09	852	
1270+03	84	1643	994	0.60	881	58
1270+04	84	1636	1665	1.02	874	
1270+05	85	1602	1272	0.79	845	57
1270+06	85	1723	1820	1.06	977	82
1270+07	85	1789	1253	0.70	1053	129
1270+08	85	1653	1078	0.65	899	
1270+09	85	1609	1124	0.70	852	17
1280+00	85	1658	1218	0.73	905	
1280+01	86	1716	1093	0.64	977	316
1280+01	86	1721	1161	0.67	983	206
1280+02	86	1717	1194	0.70	978	
1280+03	86	1609	1129	0.70	859	132
1280+04	86	1570	1418	0.90	818	
1280+05	86	1470	1178	0.80	717	199
1280+06	87	1301	1467	1.13	567	133
1280+07	87	1693	1965	1.16	959	206
1280+08	87	1684	1296	0.77	949	140
1280+09	87	1665	1914	1.15	928	170
1290+00	87	1750	1261	0.72	1025	30
1290+01	87	1515	1520	1.00	768	60
1290+02	88	1635	1215	0.74	902	180
1290+03	88	1477	1211	0.82	736	153
1290+04	88	1684	1359	0.81	957	224
1290+05	89	1636	1026	0.63	911	130
1290+06	89	1560	1620	1.04	828	160
1290+07	90	1353	1186	0.88	629	114
1290+08	90	1418	1277	0.90	690	170
1290+09	90	1550	1321	0.85	825	72
1300+00	91	1454	1431	0.98	732	52
1300+00	91	1470	1433	0.97	748	21
1300+01	91	1566	1777	1.13	849	98
1300+02	91	1446	1528	1.06	724	193
1300+03	91	1509	1783	1.18	789	134
1300+04	91	1494	1700	1.14	773	35
1300+05	91	1486	1829	1.23	765	61
1300+06	91	1533	1594	1.04	814	74
1300+07	91	1547	1121	0.72	829	105
1300+08	91	1716	1795	1.05	1020	116
1300+09	91	1516	921	0.61	796	156
1310+00	91	1592	1163	0.73	878	210

Table A2. Seismic Moduli Predicted from SPA Tests along Eastbound Right Lane (continued).

Station	AC Temp. (°F)	Phase Velocity from USW, m/sec		Velocity Ratio	AC Modulus (ksi)	IR Modulus (ksi)
		from A32	from A43			
1310+00	91	1405	1786	1.27	684	120
1310+01	91	1483	1206	0.81	762	186
1310+02	91	1656	1188	0.72	950	173
1310+03	91	1486	1307	0.88	765	214
1310+04	91	1481	1893	1.28	760	83
1310+06	92	1630	1199	0.74	928	309
1310+07	92	1529	1783	1.17	817	104
1310+08	92	1641	1785	1.09	941	303
1310+09	92	1570	1821	1.16	861	154
1320+00	92	1670	1085	0.65	975	180
1320+00	92	1568	1027	0.65	859	146
1320+01	92	1499	1894	1.26	785	153

Table A3. Seismic Moduli Predicted from SPA Tests along Westbound Left Lane.

Station	AC Temp. (°F)	Phase Velocity from USW, m/sec		Velocity Ratio	AC Modulus (ksi)	IR Modulus (ksi)
		from A32	from A43			
1324+16	69	1558			705	
1321+00	69	1539	1361	0.88	688	20
1321+00	69	1524	1369	0.90	675	18
1320+00	69	1385	1414	1.02	557	18
1320+09	69	1435	1886	1.31	598	15
1320+08	69	1420	1501	1.06	586	16
1320+07	69	1596	1424	0.89	740	
1320+06	69	1188	1044	0.88	410	
1320+05	69	1744	1739	1.00	884	19
1320+04	69	1433	1394	0.97	597	
1320+03	69	1624	1035	0.64	766	15
1320+02	69	1589	1774	1.12	734	
1320+01	69	1095	1084	0.99	348	
1310+00	69	1494	1231	0.82	649	
1310+09	69	1720	1171	0.68	860	32
1280+05	69	1556	1429	0.92	704	
1280+04	69	1576	1387	0.88	722	16
1280+03	69	1648	1731	1.05	789	17
1280+02	69	1531	1486	0.97	681	94
1280+01	69	1656	1828	1.10	797	226
1280+00	69	1301	1737	1.34	492	23
1280+09	69	1230	1452	1.18	440	123
1280+08	69	1480	1351	0.91	636	193
1280+07	69	1572	1680	1.07	718	160
1280+06	69	1589	1498	0.94	734	
1280+05	69	1677	1683	1.00	817	
1280+04	69	1727	1264	0.73	867	18
1280+03	69	1243	1057	0.85	449	
1280+02	69	1571	1458	0.93	717	19
1280+01	69	1647	1516	0.92	788	351
1270+00	69	1488	1749	1.18	643	20
1270+09	69	1539	1651	1.07	688	163
1270+08	69	1539	1387	0.90	688	229
1270+07	69	1493	1359	0.91	648	18
1270+06	69	1581	1576	1.00	726	160
1270+05	69	1695	1630	0.96	835	219
1270+04	69	1583	1195	0.75	728	259
1270+03	69	1740	1848	1.06	880	48
1270+02	69	1565	1512	0.97	712	216
1270+01	69	1725	1625	0.94	865	344
1260+00	69	1531	1792	1.17	681	18
1260+09	69	1638	1405	0.86	780	263
1260+08	69	1613	1719	1.07	756	25
1260+07	69	1325	1652	1.25	510	247
1260+06	69	1611	1711	1.06	754	18
1260+05	69	1558	1556	1.00	705	18

Table A3. Seismic Moduli Predicted from SPA Tests along Westbound Left Lane (continued)

Station	AC Temp. (°F)	Phase Velocity from USW, m/sec		Velocity Ratio	AC Modulus (ksi)	IR Modulus (ksi)
		from A32	from A43			
1260+04	69	1624	1589	0.98	766	204
1260+03	69	1511	1301	0.86	663	138
1260+02	69	1509	1232	0.82	662	19
1260+01	69	1582	1391	0.88	727	
1250+00	69	1387	1769	1.28	559	17
1250+09	69	1505	1331	0.88	658	16
1250+08	69	1757	1907	1.09	897	
1250+07	69	1713	1611	0.94	853	
1250+06	69	1629	1803	1.11	771	304
1250+02	69	1742	1722	0.99	882	
1250+01	69	1569	1647	1.05	715	21
1240+00	69	1809	1735	0.96	951	16
1240+09	69	1617	1703	1.05	760	17
1240+08	69	1543	1266	0.82	692	23
1240+07	69	1667	1647	0.99	808	
1240+06	69	1436	2015	1.40	599	21
1240+05	69	1813	1069	0.59	955	14
1240+04	69	1699	1665	0.98	839	16
1240+03	69	1617	1456	0.90	760	
1240+02	69	1686	1634	0.97	826	16
1240+01	69	1472	1219	0.83	630	
1230+00	69	1501	1760	1.17	655	16
1230+09	69	1699	1495	0.88	839	286
1230+08	69	1699	1541	0.91	839	131
1230+07	69	1734	1075	0.62	874	351
1230+06	69	1570	1568	1.00	716	114
1230+05	69	1648	1072	0.65	789	163
1230+04	69	1621	1395	0.86	764	141
1230+03	69	1611	1866	1.16	754	146
1230+02	69	1658	1477	0.89	799	147
1230+01	69	1620	1351	0.83	763	166
1220+00	69	1573	1314	0.84	719	516
1220+09	69	1425	1332	0.93	590	22
1220+08	69	1468	1456	0.99	626	144
1220+07	69	1543	1535	0.99	692	216
1220+06	69	1828	2112	1.16	971	299
1220+05	69	1725	1911	1.11	865	263
1220+04	69	1675	1014	0.61	815	
1220+03	69	1707	1759	1.03	847	24
1220+02	69	1680	1722	1.03	820	15
1220+01	69	1611	1265	0.79	754	
1210+00	69	1601	1666	1.04	745	92
1210+09	69	1662	1675	1.01	803	
1210+08	69	1721	1698	0.99	861	

Table A3. Seismic Moduli Predicted from SPA Tests along Westbound Left Lane (continued)

Station	AC Temp. (°F)	Phase Velocity from USW, m/sec		Velocity Ratio	AC Modulus (ksi)	IR Modulus (ksi)
		from A32	from A43			
1210+07	69	1794	1554	0.87	935	25
1210+06	69	1373	1740	1.27	548	137
1210+05	69	1639	1624	0.99	781	
1210+04	69	1489	1647	1.11	644	18
1210+03	69	1691	1622	0.96	831	
1210+02	69	1756	1368	0.78	896	
1210+01	69	1412	1792	1.27	579	21
1200+00	69	1452	1666	1.15	613	
1200+09	69	1681	1564	0.93	821	
1200+08	69	1658	1736	1.05	799	19
1200+07	69	1612	1649	1.02	755	
1200+06	69	1745	1779	1.02	885	161
1200+05	69	1606	1635	1.02	749	
1200+04	69	1660	1613	0.97	801	
1200+03	69	1336	1605	1.20	519	
1200+02	69	1511	1436	0.95	663	23
1190+00	69	1655	1876	1.13	796	319
1190+09	69	1616	1590	0.98	759	227
1190+08	69	1472	1369	0.93	630	166
1190+07	69	1552	1409	0.91	700	189
1190+06	69	1610	1351	0.84	753	266
1190+05	69	1626	1438	0.88	768	113
1190+04	69	1714	1576	0.92	854	106
1190+03	69	1415	1566	1.11	582	120
1190+02	69	1578	1724	1.09	724	274
1190+01	69	1684	1852	1.10	824	353
1180+00	69	1524	1578	1.04	675	357
1180+09	69	1267	1222	0.96	466	210
1180+08	69	1592	1280	0.80	736	241
1180+07	69	1566	1326	0.85	713	193
1180+06	69	1433	1576	1.10	597	254
1180+05	69	1636	1105	0.68	778	
1180+04	69	1528	1313	0.86	678	194
1180+03	69	1506	1215	0.81	659	154
1180+02	69	1268	1229	0.97	467	132
1170+00	69	1636	1099	0.67	778	107
1170+09	69	1631	1517	0.93	773	366
1170+08	69	1663	1804	1.08	804	31
1168+00	69	1473	1591	1.08	630	220
1170+07	69	1633	1643	1.01	775	181

Table A4. Seismic Moduli Predicted from SPA Tests along Westbound Right Lane.

Station	AC Temp. (°F)	Phase Velocity from USW, m/sec		Velocity Ratio	AC Modulus (ksi)	IR Modulus (ksi)
		from A32	from A43			
1321+00	73	1807	1551	0.86	977	39
1320+00	73	1800	603	0.34	970	151
1310+09	73	1678	1712	1.02	843	246
1310+08	73	1415	2120	1.50	599	81
1310+07	73	1623	1500	0.92	789	99
1310+06	73	1764	1763	1.00	931	161
1310+05	73	1754	1794	1.02	921	16
1310+04	73	1494	1473	0.99	668	450
1310+03	73	1670	1614	0.97	835	
1310+02	73	1477	1724	1.17	653	330
1310+01	73	1669	1644	0.99	834	84
1310+00	73	1394	1324	0.95	582	223
1310+09	73	1640	1972	1.20	805	224
1310+08	73	1715	1901	1.11	880	117
1310+07	73	1745	1715	0.98	912	35
1310+06	73	1687	1622	0.96	852	120
1310+05	73	1812	1820	1.00	983	94
1310+04	73	1829	1776	0.97	1001	112
1310+03	73	1859	1832	0.99	1035	176
1310+02	73	1745	1761	1.01	912	191
1310+01	73	1890	1888	1.00	1069	62
1300+00	73	1814	1882	1.04	985	200
1300+09	73	1590	1801	1.13	757	122
1300+08	73	1886	1575	0.84	1065	191
1300+07	73	1844	1939	1.05	1018	
1300+06	73	1746	2032	1.16	913	39
1300+05	73	1636	1570	0.96	801	269
1300+04	73	1572	1777	1.13	740	207
1300+01	73	1764	2037	1.15	931	317
1290+00	73	1724	1836	1.06	890	823
1290+09	73	1459	1790	1.23	637	259
1290+08	73	1711	1814	1.06	876	23
1290+07	73	1779	1848	1.04	947	16
1290+06	73	1663	1858	1.12	828	306
1290+05	73	1494	1782	1.19	668	254
1290+04	73	1733	1928	1.11	899	346
1290+03	73	1757	1669	0.95	924	136
1290+02	73	1808	1950	1.08	979	59
1290+01	73	1881	1865	0.99	1059	63
1280+00	73	1503	1995	1.33	676	98
1280+09	73	1425	1567	1.10	608	706
1280+08	73	1653	2018	1.22	818	
1280+07	73	1558	1674	1.07	727	816
1280+05	73	1587	1271	0.80	754	
1280+04	73	1571	1880	1.20	739	203
1280+03	73	1610	1688	1.05	776	120

Table A4. Seismic Moduli Predicted from SPA Tests along Westbound Right Lane (continued).

Station	AC Temp. (°F)	Phase Velocity from USW, m/sec		Velocity Ratio	AC Modulus (ksi)	IR Modulus (ksi)
		from A32	from A43			
1280+02	73	1900	1788	0.94	1081	
1280+01	73	1893	1968	1.04	1073	
1270+00	73	1753	1718	0.98	920	246
1270+09	73	1746	1779	1.02	913	241
1270+08	73	1728	1914	1.11	894	
1270+07	73	1834	1914	1.04	1007	266
1270+06	73	1821	1990	1.09	993	
1270+05	73	1787	1984	1.11	956	
1270+04	73	1666	1781	1.07	831	16
1270+03	73	1685	1994	1.18	850	22
1270+02	73	1693	1609	0.95	858	
1270+01	73	1814	1973	1.09	985	246
1260+00	73	1604	1761	1.10	770	35
1260+09	73	1748	1708	0.98	915	35
1260+08	73	1700	1653	0.97	865	31
1260+07	73	1773	1900	1.07	941	283
1260+06	73	1729	1833	1.06	895	23
1260+05	73	1687	1660	0.98	852	88
1260+04	73	1816	1828	1.01	987	
1260+03	73	1783	1645	0.92	952	20
1260+02	73	1822	1750	0.96	994	31
1260+02	73	1835	1783	0.97	1008	
1260+01	73	1874	1804	0.96	1051	
1250+00	73	1544	1724	1.12	714	
1250+09	73	1754	1539	0.88	921	
1250+08	73	1857	1909	1.03	1032	
1250+07	73	1850	1710	0.92	1025	110
1250+06	73	1602	1799	1.12	768	183
1250+02	73	1659	1676	1.01	824	24
1250+01	73	1826	1350	0.74	998	123
1240+00	73	1622	1738	1.07	788	
1240+09	73	1855	1857	1.00	1030	128
1240+08	73	1502	1481	0.99	675	55
1240+07	73	1613	1939	1.20	779	
1240+06	73	1513	1643	1.09	685	
1240+05	73	1776	1601	0.90	944	20
1240+04	73	1573	1975	1.26	741	25
1240+03	73	1660	1605	0.97	825	
1240+02	73	1460	1894	1.30	638	
1240+01	73	1748	1543	0.88	915	
1230+00	73	1338	1632	1.22	536	17
1230+09	73	1706	1866	1.09	871	
1230+08	73	1749	1819	1.04	916	19
1230+07	73	1598	1861	1.16	764	

Table A4. Seismic Moduli Predicted from SPA Tests along Westbound Right Lane (continued).

Station	AC Temp. (°F)	Phase Velocity from USW, m/sec		Velocity Ratio	AC Modulus (ksi)	IR Modulus (ksi)
		from A32	from A43			
1230+06	73	1675	1763	1.05	840	20
1230+05	73	1618	1296	0.80	784	19
1230+04	73	1811	1688	0.93	982	
1230+03	73	1584	1566	0.99	751	230
1230+02	73	1245	1463	1.18	464	216
1230+01	73	1573	1670	1.06	741	204
1220+00	73	1583	1559	0.98	750	20
1220+09	73	1550	1512	0.98	719	14
1220+08	73	1460	1936	1.33	638	
1220+07	73	1895	1913	1.01	1075	23
1220+06	73	1666	1832	1.10	831	
1220+05	73	1732	1826	1.05	898	19
1220+04	73	1859	1734	0.93	1035	128
1220+03	73	1602	1036	0.65	768	
1220+02	73	1616	1642	1.02	782	58
1220+01	73	1514	1508	1.00	686	23
1210+00	73	1595	1426	0.89	762	17
1210+09	73	1692	1586	0.94	857	
1210+08	73	1309	1382	1.06	513	
1210+07	73	1625	1646	1.01	790	
1210+06	73	1684	1331	0.79	849	17
1210+05	73	1659	1670	1.01	824	85
1210+04	73	1508	1352	0.90	681	21
1210+03	73	1618	1661	1.03	784	
1210+02	73	1645	1747	1.06	810	118
1210+01	73	1549	1744	1.13	718	21
1200+00	73	1837	1187	0.65	1010	
1200+09	73	1478	1345	0.91	654	
1200+08	73	1840	1844	1.00	1013	
1200+07	73	1626	1561	0.96	791	20
1200+06	73	1656	1739	1.05	821	16
1200+05	73	1590	1676	1.05	757	
1200+04	73	1704	1553	0.91	869	
1200+03	73	1670	1757	1.05	835	54
1200+02	73	1756	1723	0.98	923	221
1200+01	73	1743	1742	1.00	909	72
1190+00	73	1665	1914	1.15	830	
1190+09	73	1765	2031	1.15	933	156
1190+08	73	1505	1572	1.04	678	
1190+07	73	1872	1970	1.05	1049	72
1190+06	73	1653	1236	0.75	818	29
1190+05	73	1664	1849	1.11	829	30
1190+04	73	1459	1433	0.98	637	17
1190+03	73	1761	1804	1.02	928	

Table A4. Seismic Moduli Predicted from SPA Tests along Westbound Right Lane (continued).

Station	AC Temp. (°F)	Phase Velocity from USW, m/sec		Velocity Ratio	AC Modulus (ksi)	IR Modulus (ksi)
		from A32	from A43			
1190+02	73	1383	1733	1.25	573	24
1190+01	73	1540	1237	0.80	710	32
1180+00	73	1369	1102	0.80	561	19
1180+09	73	1323	1085	0.82	524	
1180+08	73	1643	1534	0.93	808	28
1180+07	73	1593	1504	0.94	760	
1180+06	73	1782	1639	0.92	951	
1180+05	73	1591	1700	1.07	758	237
1180+02	73	1625	1273	0.78	790	24
1180+01	73	1622	1434	0.88	788	16
1170+00	73	1607	1352	0.84	773	14
1170+09	73	1549	1628	1.05	718	24
1170+08	73	1521	1489	0.98	693	25
1170+07	73	1654	1542	0.93	819	171
1170+06	73	1589	1701	1.07	756	24
1170+05	73	1625	1622	1.00	790	327
1170+04	73	1650	1709	1.04	815	240
1170+03	73	1738	1839	1.06	904	16
1170+02	73	1623	1885	1.16	789	135
1170+01	73	1449	1498	1.03	629	23
1160+00	73	1693	1726	1.02	858	69
1160+09	73	1786	1789	1.00	955	
1160+08	73	1863	2066	1.11	1039	17
1160+07	73	1584	1529	0.97	751	114
1160+06	73	1791	2070	1.16	960	25
1160+05	73	1564	1718	1.10	732	16
1160+04	73	1629	1627	1.00	794	84
1160+03	73	1689	1602	0.95	854	93
1160+02	73	1842	1845	1.00	1016	126
1160+01	73	1547	1288	0.83	716	17
1150+00	73	1496	1545	1.03	670	48
1150+09	73	1399	1165	0.83	586	15
1150+08	73	1529	1391	0.91	700	187
1150+07	73	1484	1439	0.97	659	169
1150+06	73	1341	1599	1.19	538	163
1150+05	73	1455	1205	0.83	634	100
1150+04	73	1723	1981	1.15	889	143
1150+03	73	1566	1521	0.97	734	221
1150+02	73	1651	1653	1.00	816	210
1140+00	73	1485	1435	0.97	660	
1140+09	73	1724	1481	0.86	890	
1140+08	73	1782	2067	1.16	951	15
1140+07	73	1819	1897	1.04	990	21
1140+06	73	1809	1992	1.10	980	
1140+05	73	1827	2299	1.26	999	18

APPENDIX B
GPR TEST DATA

This appendix presents color-coded representations of the GPR data collected by TTI researchers along the I-20 overlay project near Marshall, Texas. The reflections from the layer interfaces detected from GPR are labeled in the figures. Note that the surface reflection has been removed, and only the interfaces appearing below the surface are shown.

The color bar at the left side of each figure shows the color coding of the reflection amplitudes. These amplitudes are expressed in volts and range from ±1 volt. Voltages around 1 volt are coded red, while voltages around -1 volt are coded blue. Amplitudes between these limits are assigned the color shown on the bar. The depth scale at the right side of each figure gives the predicted depth of each interface detected by GPR. From this scale, one can determine the thickness of each layer.

At the bottom of each figure is the distance scale expressed in miles and feet. The distance corresponding to each GPR trace is recorded during the measurement. The upper number on the distance scale shows the miles traversed, while the lower number is the distance traveled in feet since the last mile. For example, 6287 ft corresponds to 1 mile and 1007 ft. Also shown above the distance scale is the predicted dielectric profile of the existing AC surface mix on the lane surveyed. This profile may be used to locate possible changes in the surface mix along the length surveyed.

The figures included in this appendix therefore provide all relevant information from the GPR testing. Each figure shows:

- the variation of the pavement layering along the length surveyed, as determined from radar;
- the amplitudes of the reflections from the layer interfaces;
- the thickness of each layer; and
- the computed dielectric values of the surface material.

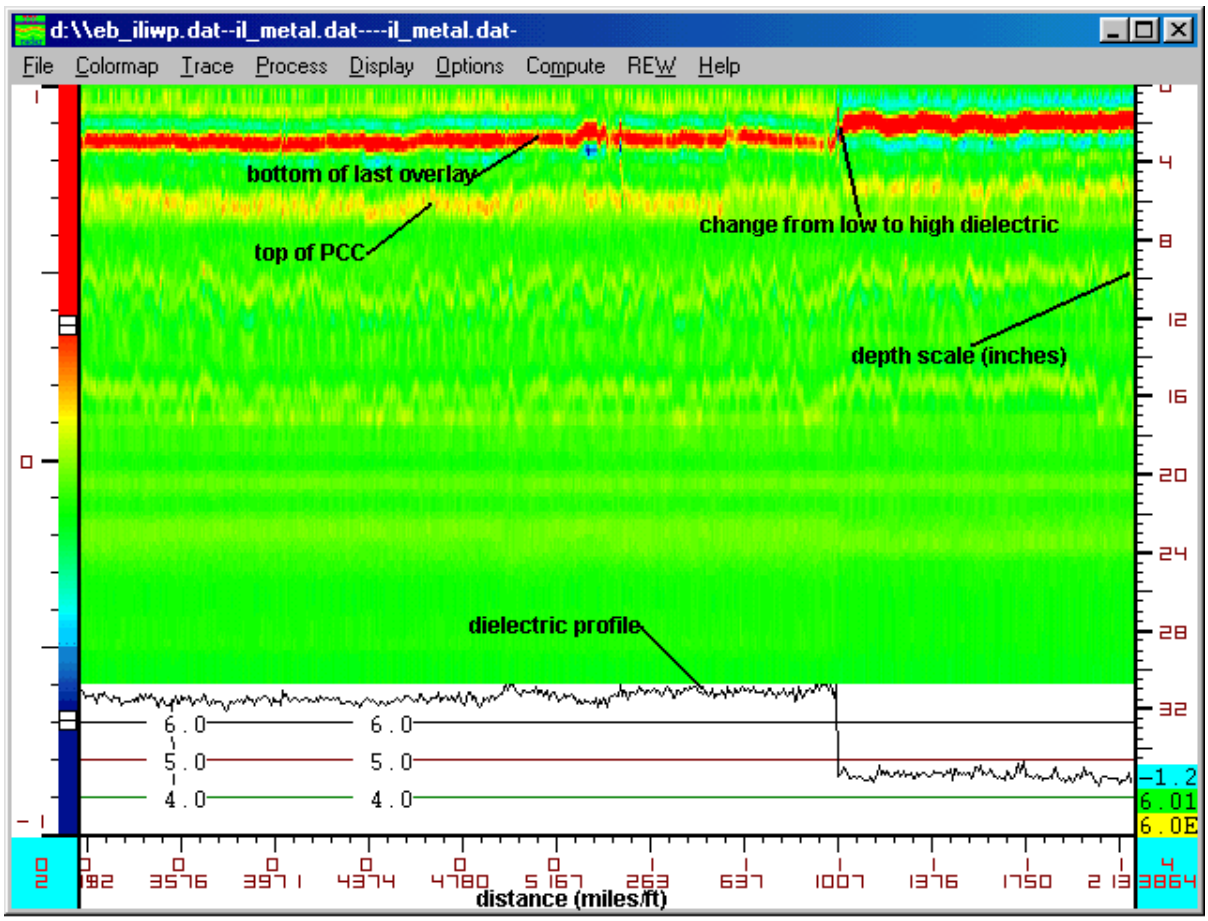

Figure B1. GPR Data Collected along Eastbound Inside Lane of I-20 Project (1/4).

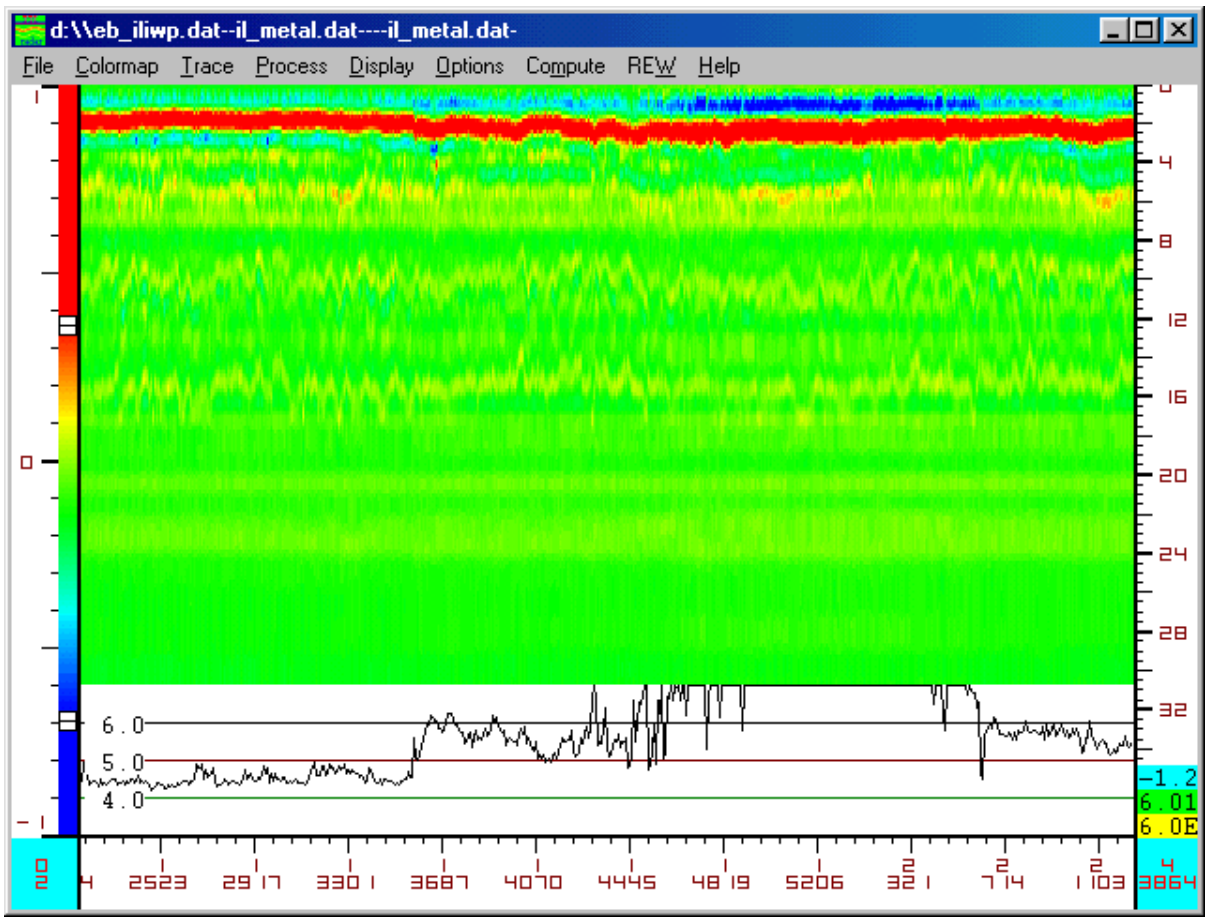

Figure B2. GPR Data Collected along Eastbound Inside Lane of I-20 Project (2/4).

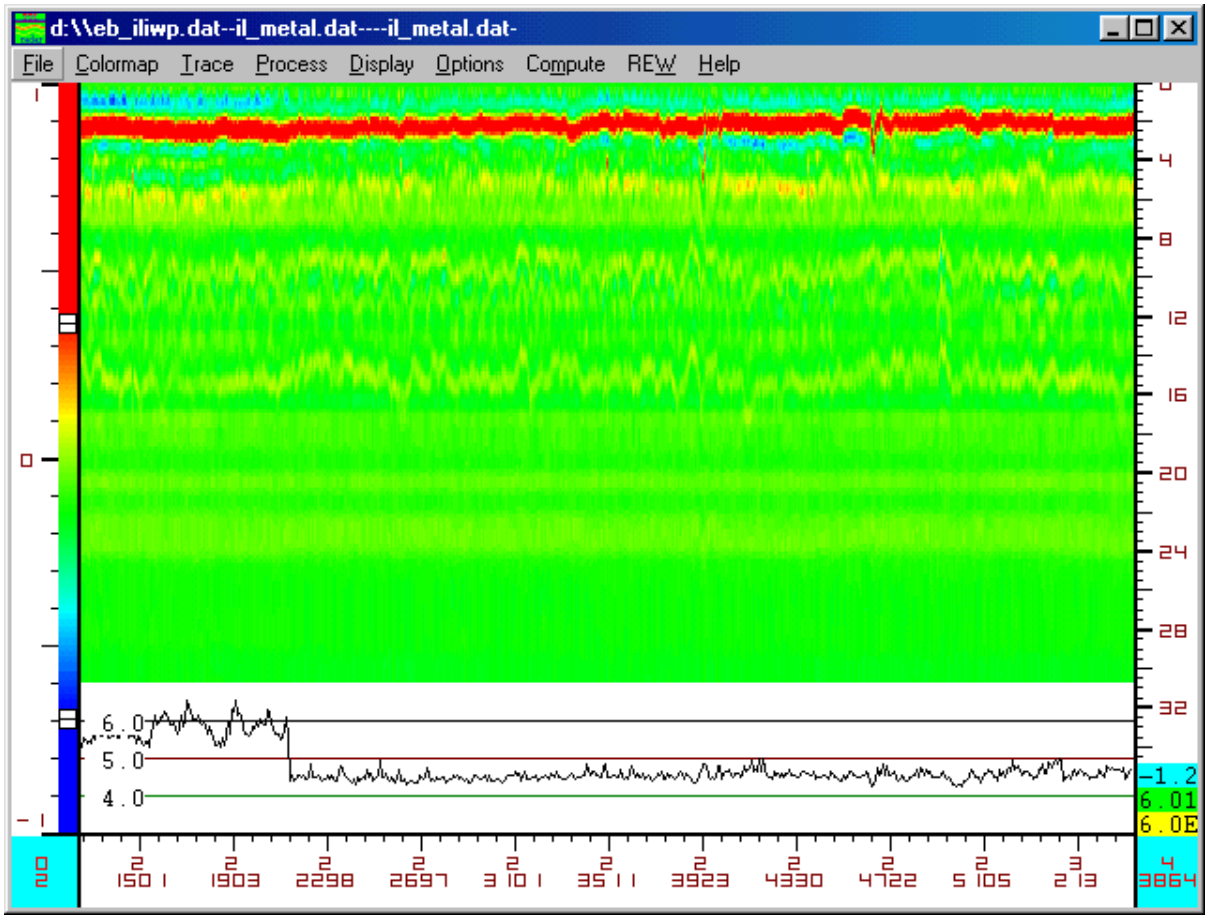

Figure B3. GPR Data Collected along Eastbound Inside Lane of I-20 Project (3/4).

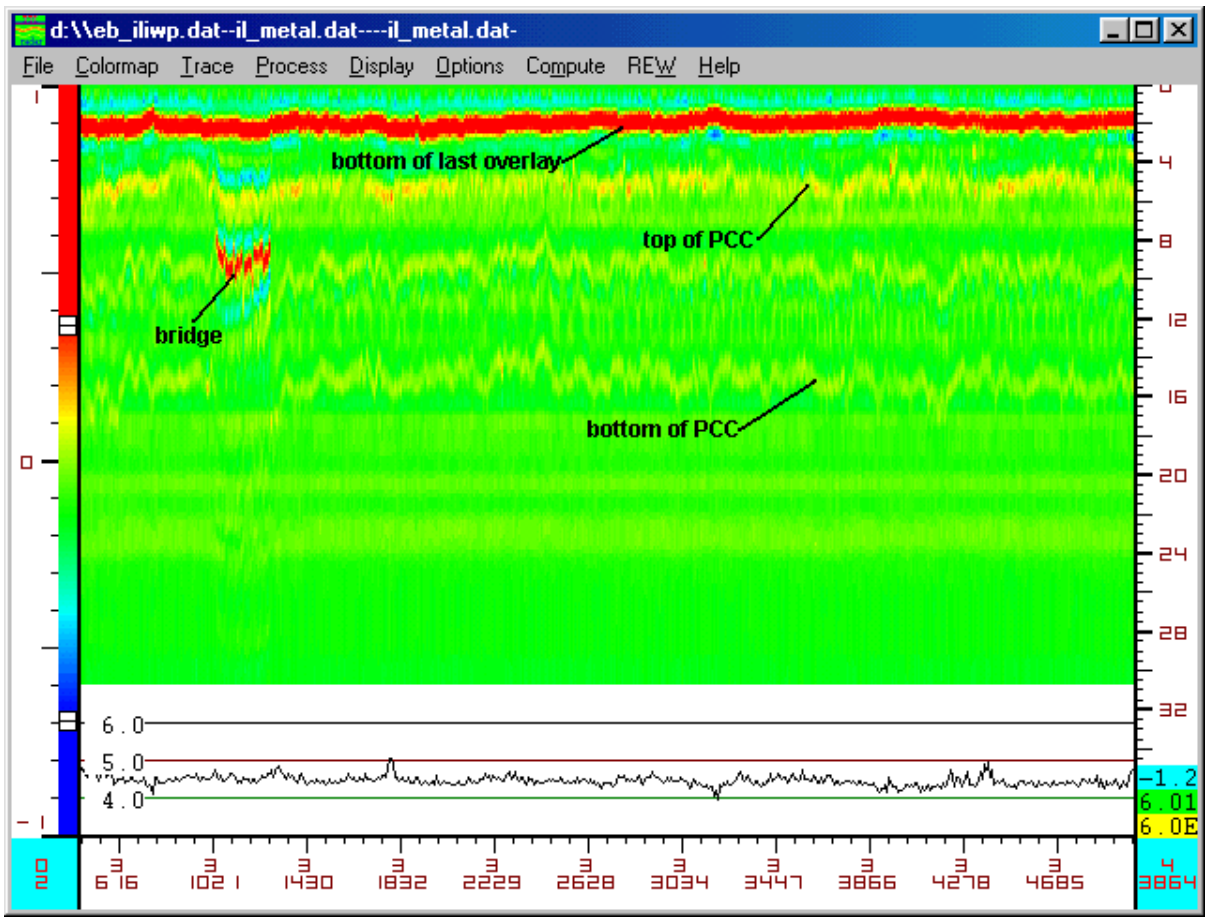

Figure B4. GPR Data Collected along Eastbound Inside Lane of I-20 Project (4/4).

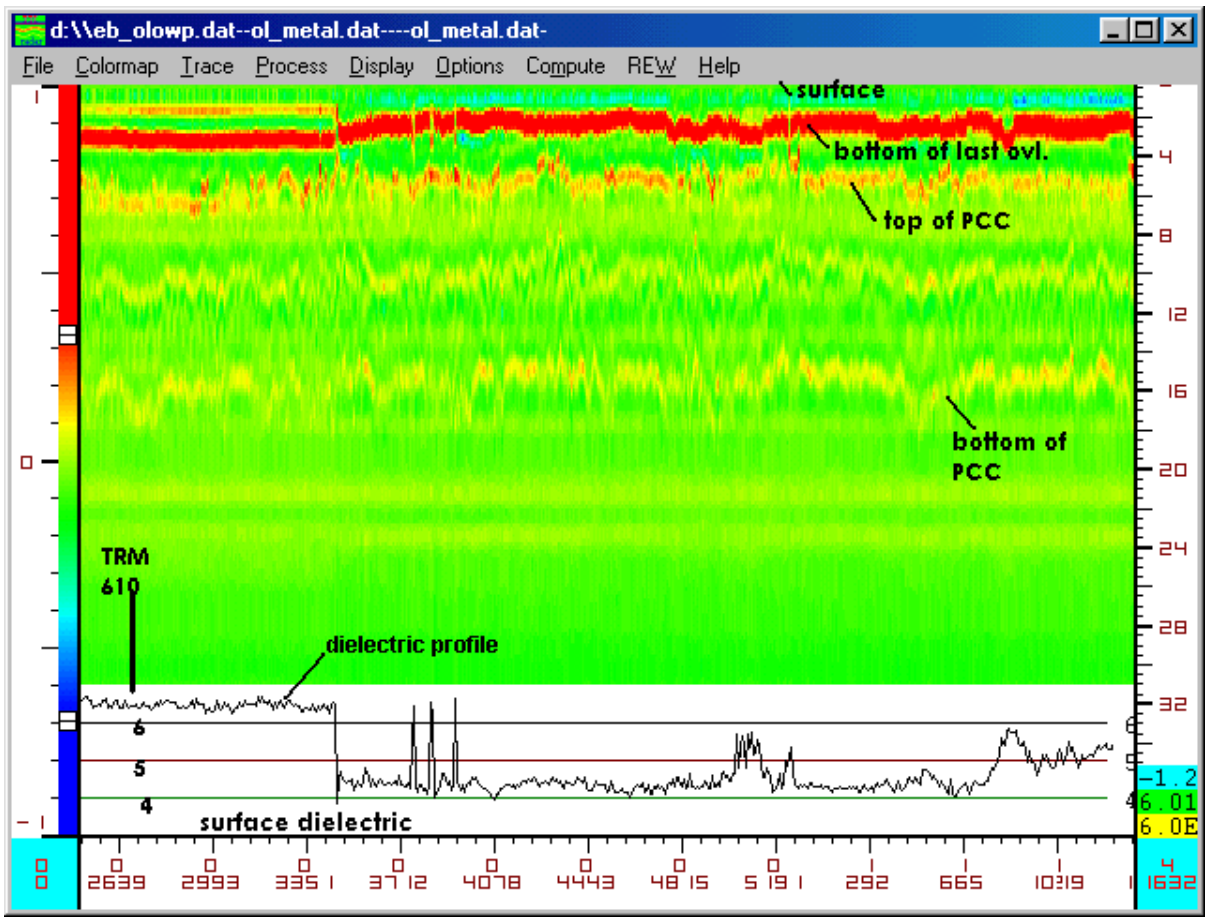

Figure B5. GPR Data Collected along Eastbound Outside Lane of I-20 Project (1/4).

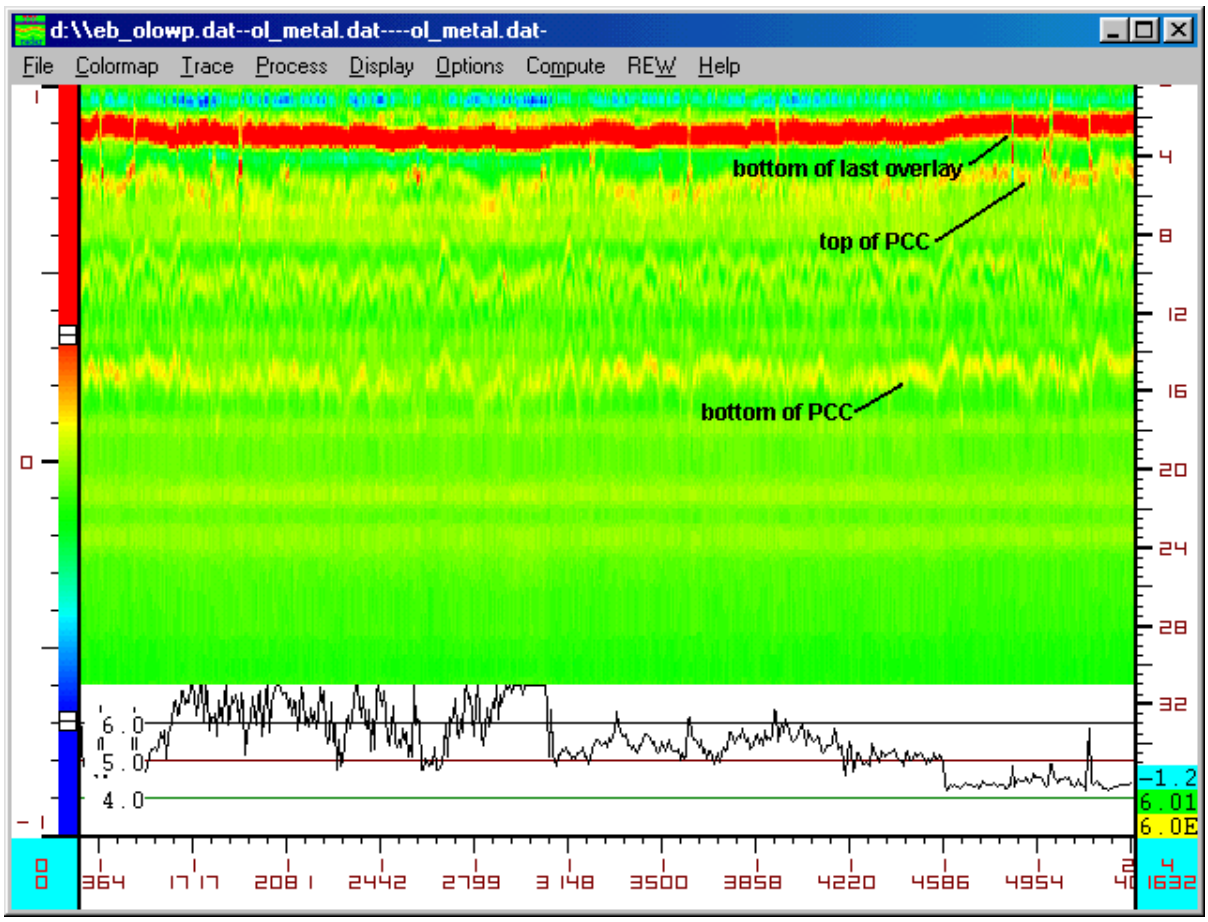

Figure B6. GPR Data Collected along Eastbound Outside Lane of I-20 Project (2/4).

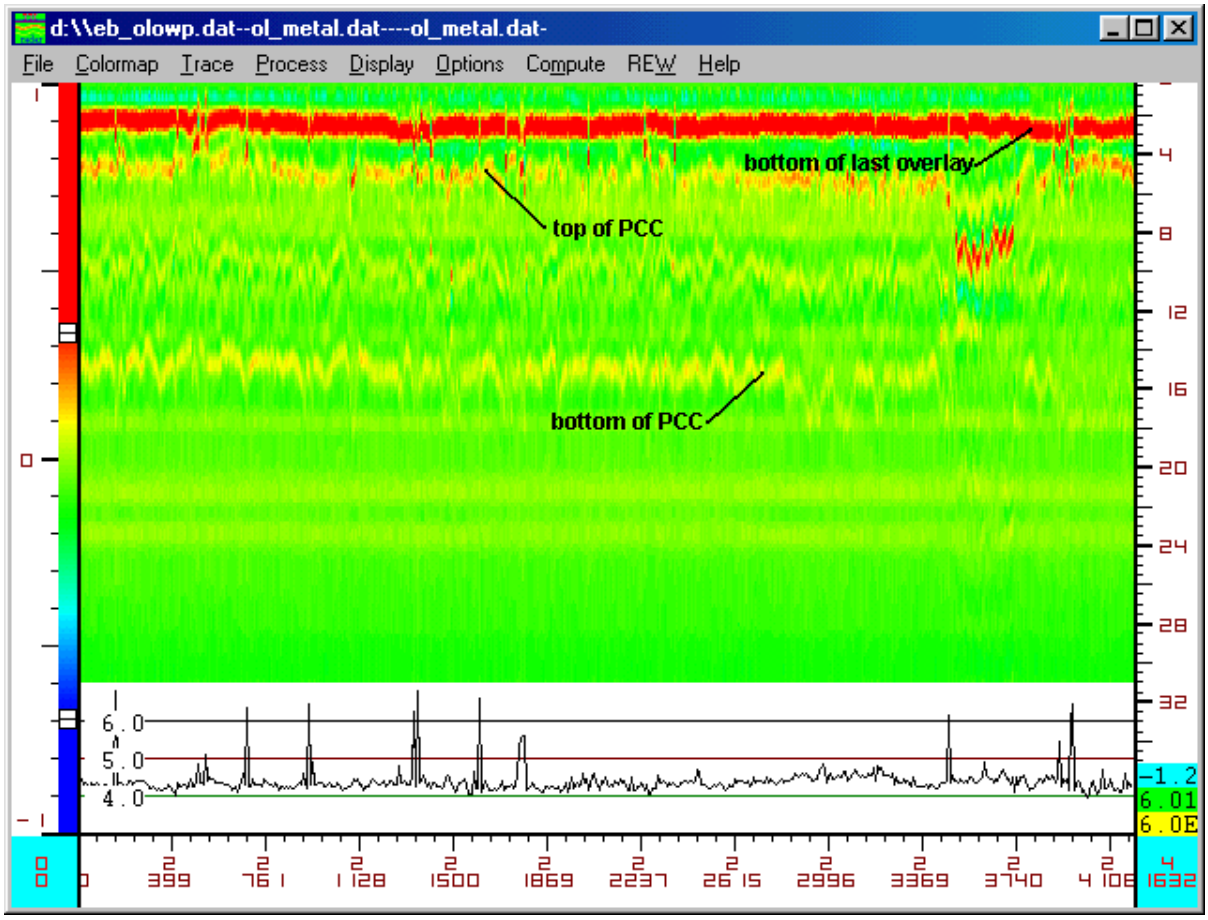

Figure B7. GPR Data Collected along Eastbound Outside Lane of I-20 Project (3/4).

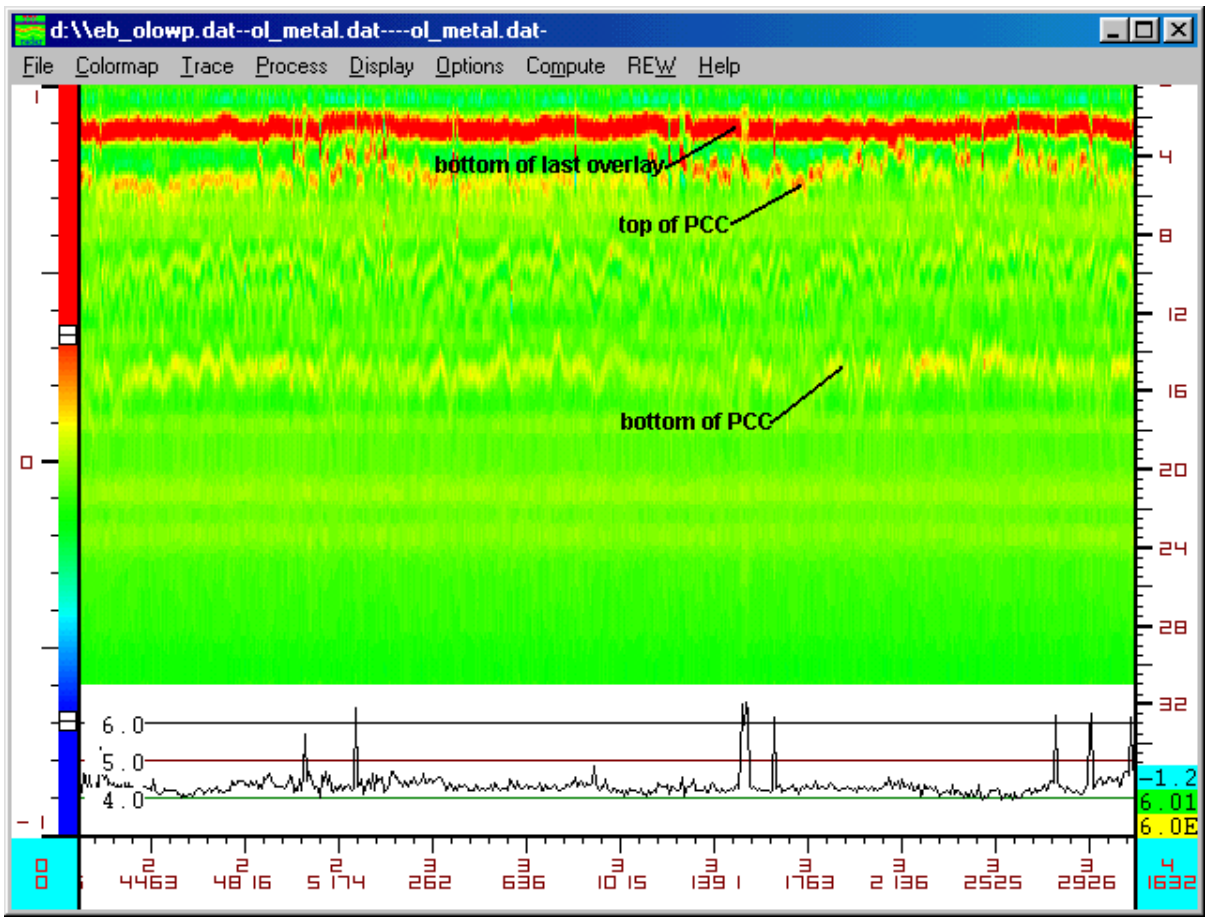

Figure B8. GPR Data Collected along Eastbound Outside Lane of I-20 Project (4/4).

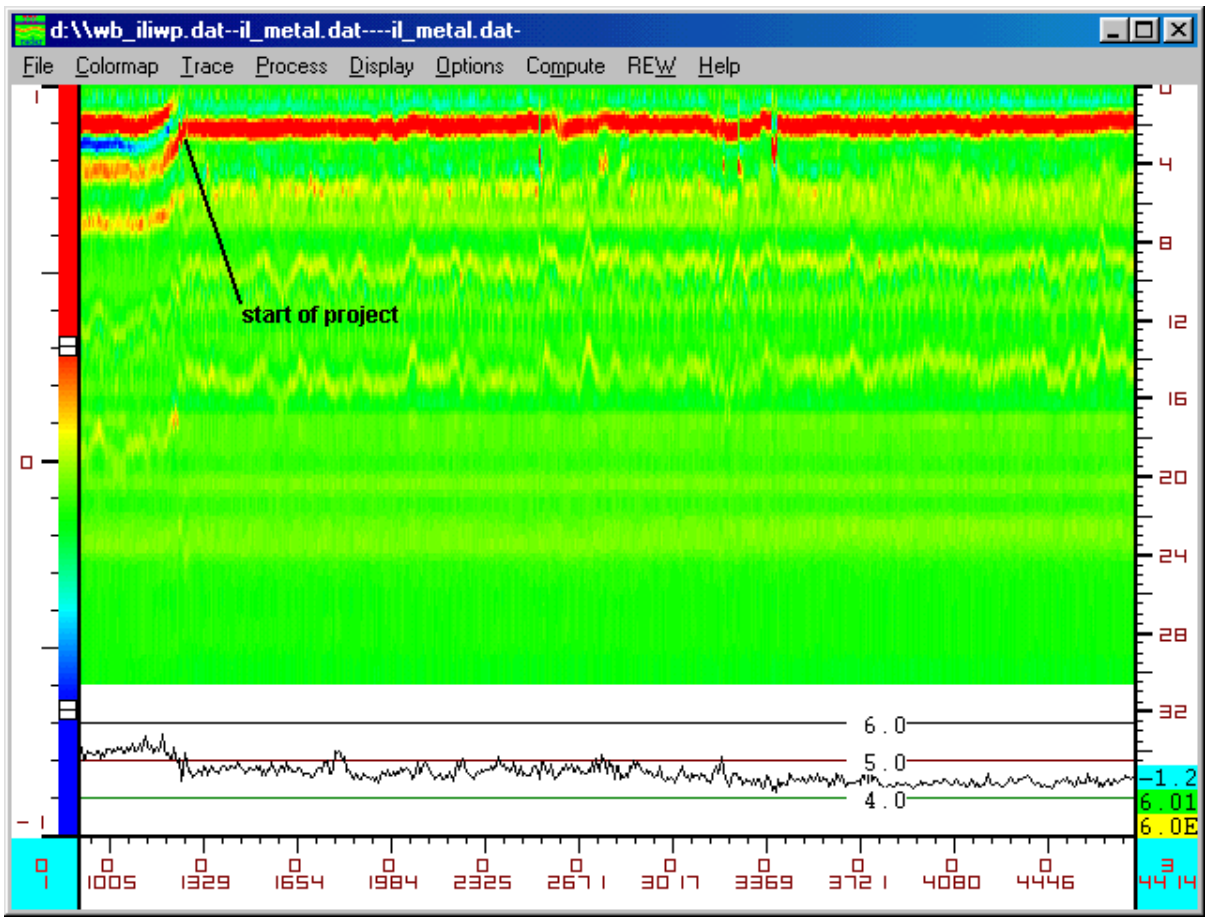

Figure B9. GPR Data Collected along Westbound Inside Lane of I-20 Project (1/4).

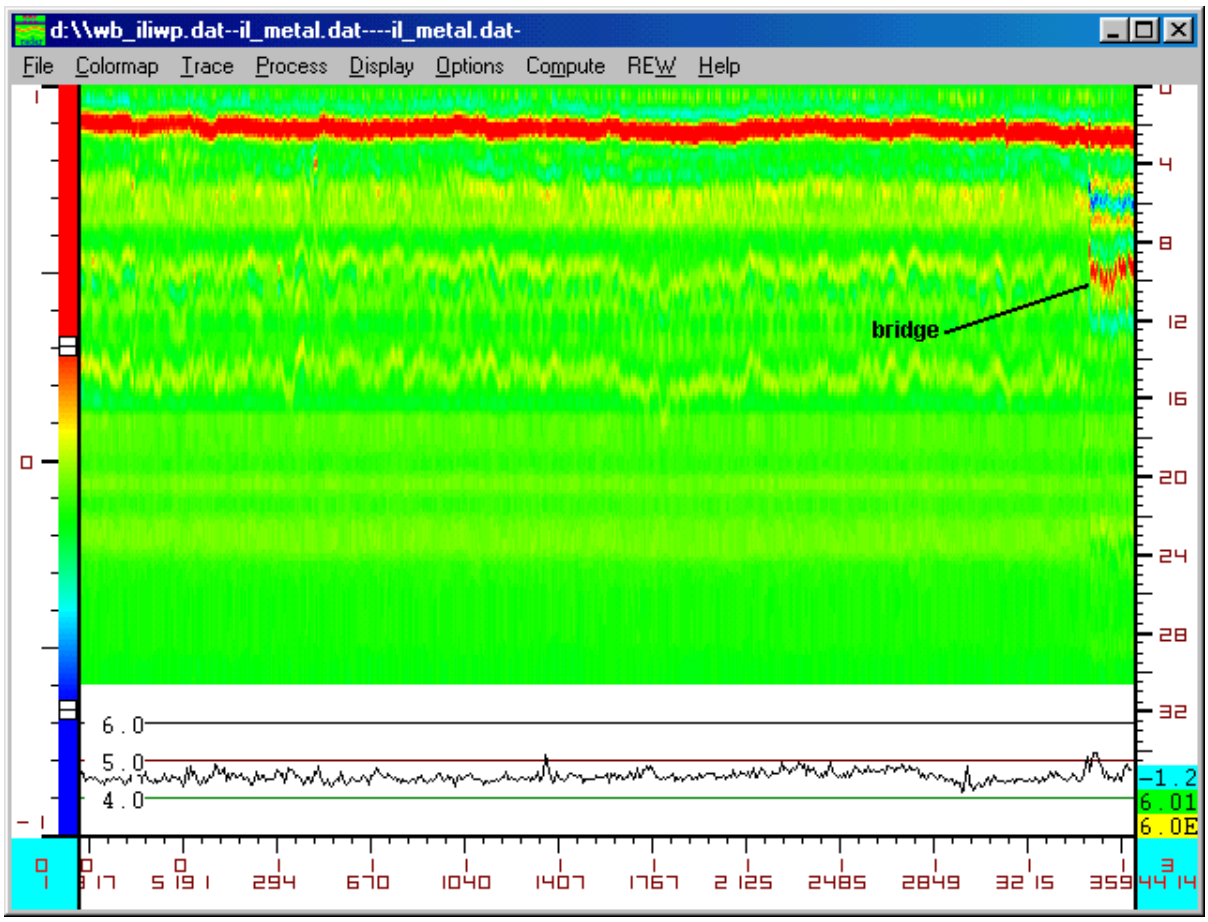

Figure B10. GPR Data Collected along Westbound Inside Lane of I-20 Project (2/4).

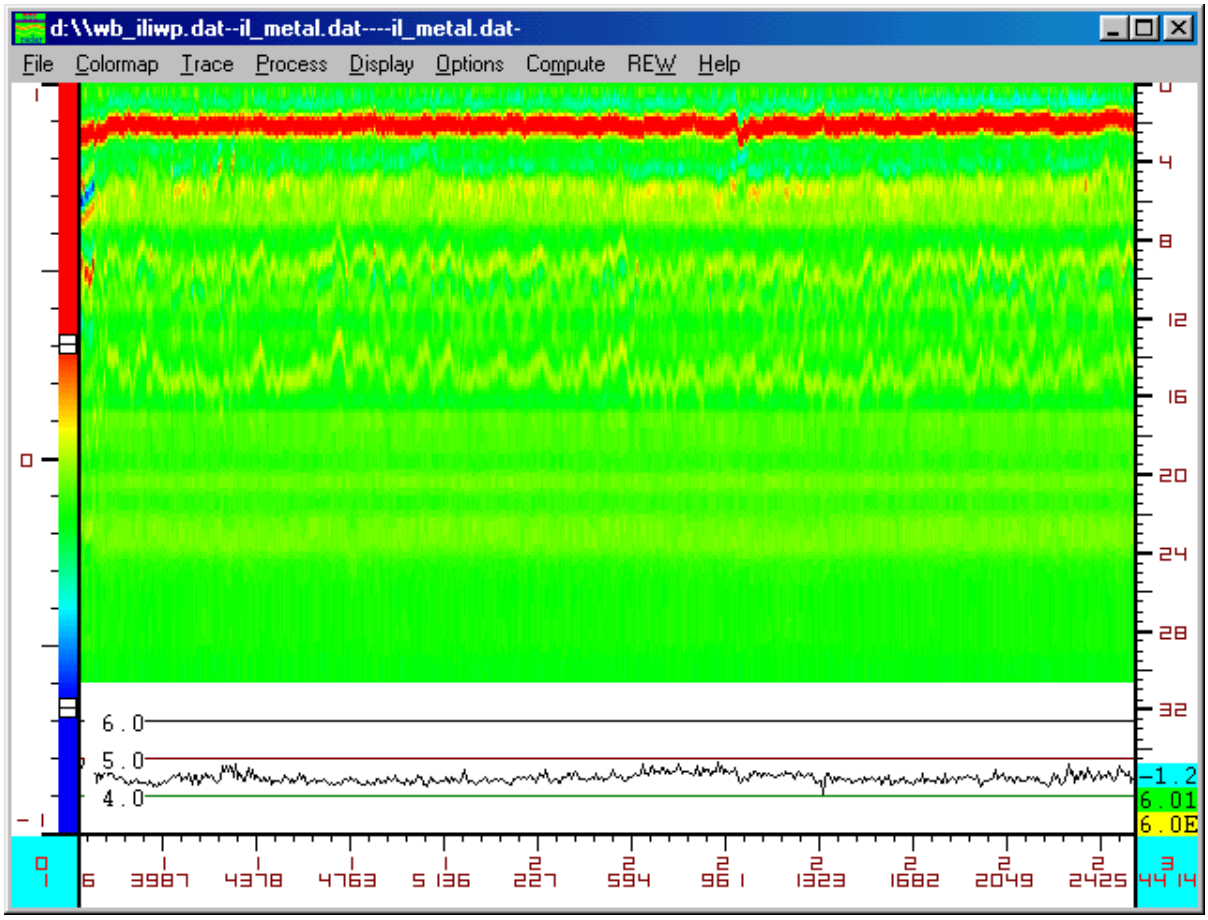

Figure B11. GPR Data Collected along Westbound Inside Lane of I-20 Project (3/4).

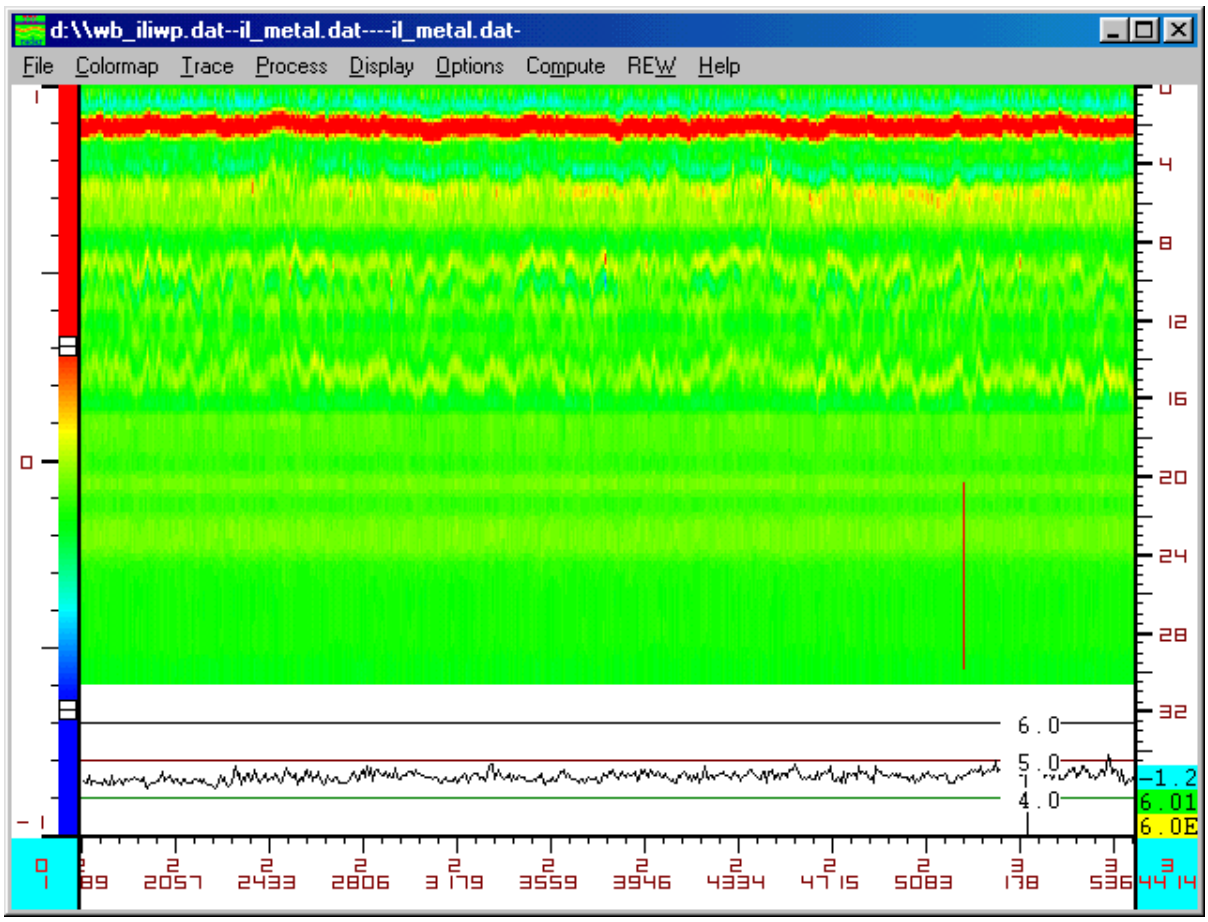

Figure B12. GPR Data Collected along Westbound Inside Lane of I-20 Project (4/4).

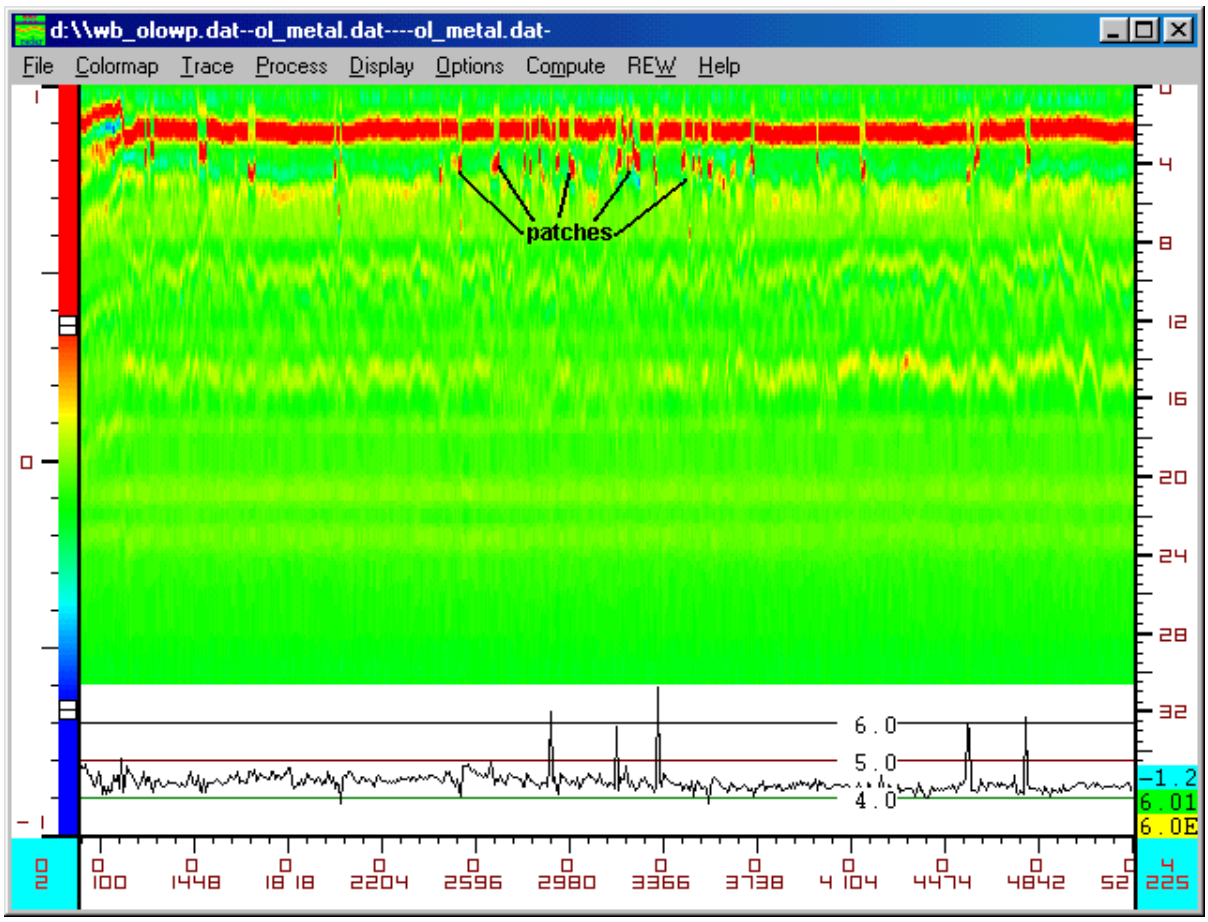

Figure B13. GPR Data Collected along Westbound Outside Lane of I-20 Project (1/4).

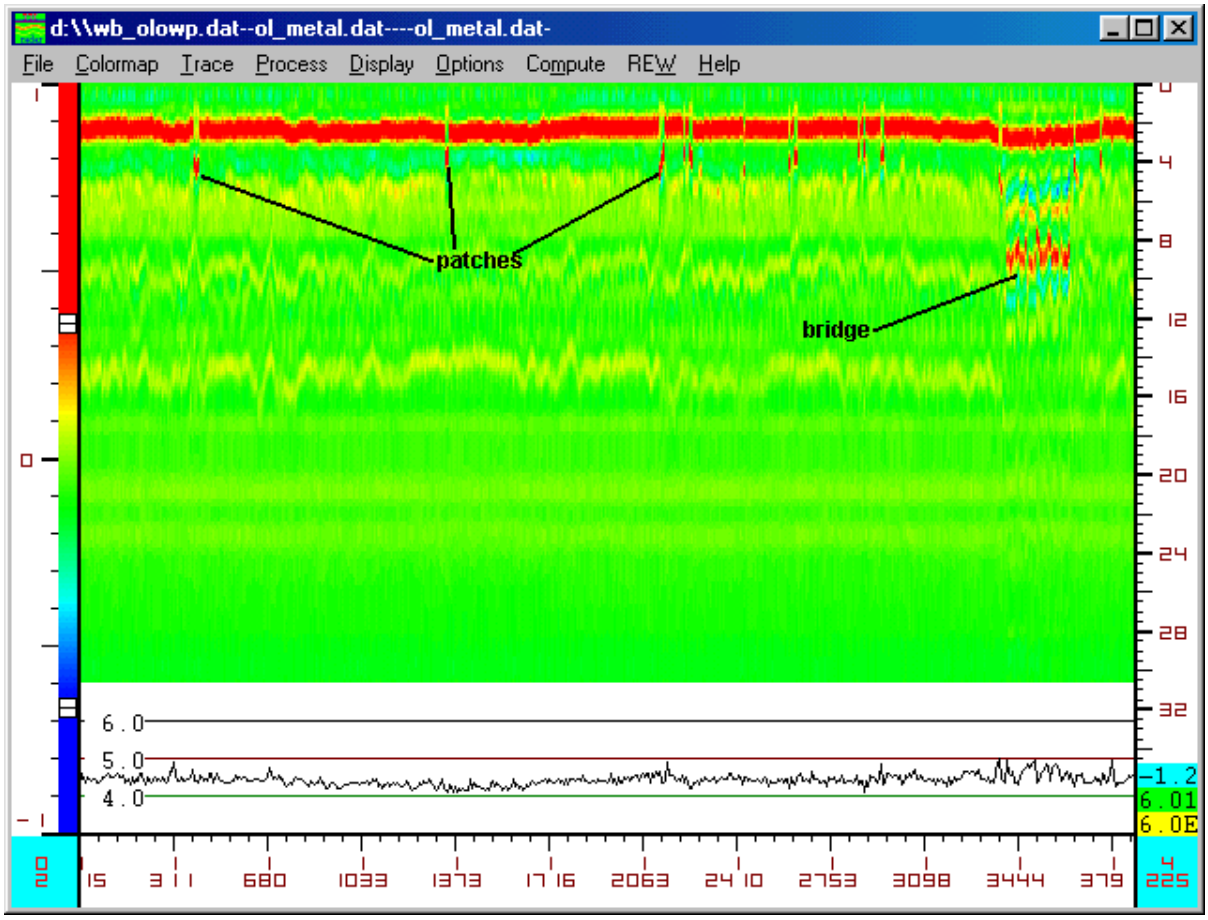

Figure B14. GPR Data Collected along Westbound Outside Lane of I-20 Project (2/4).

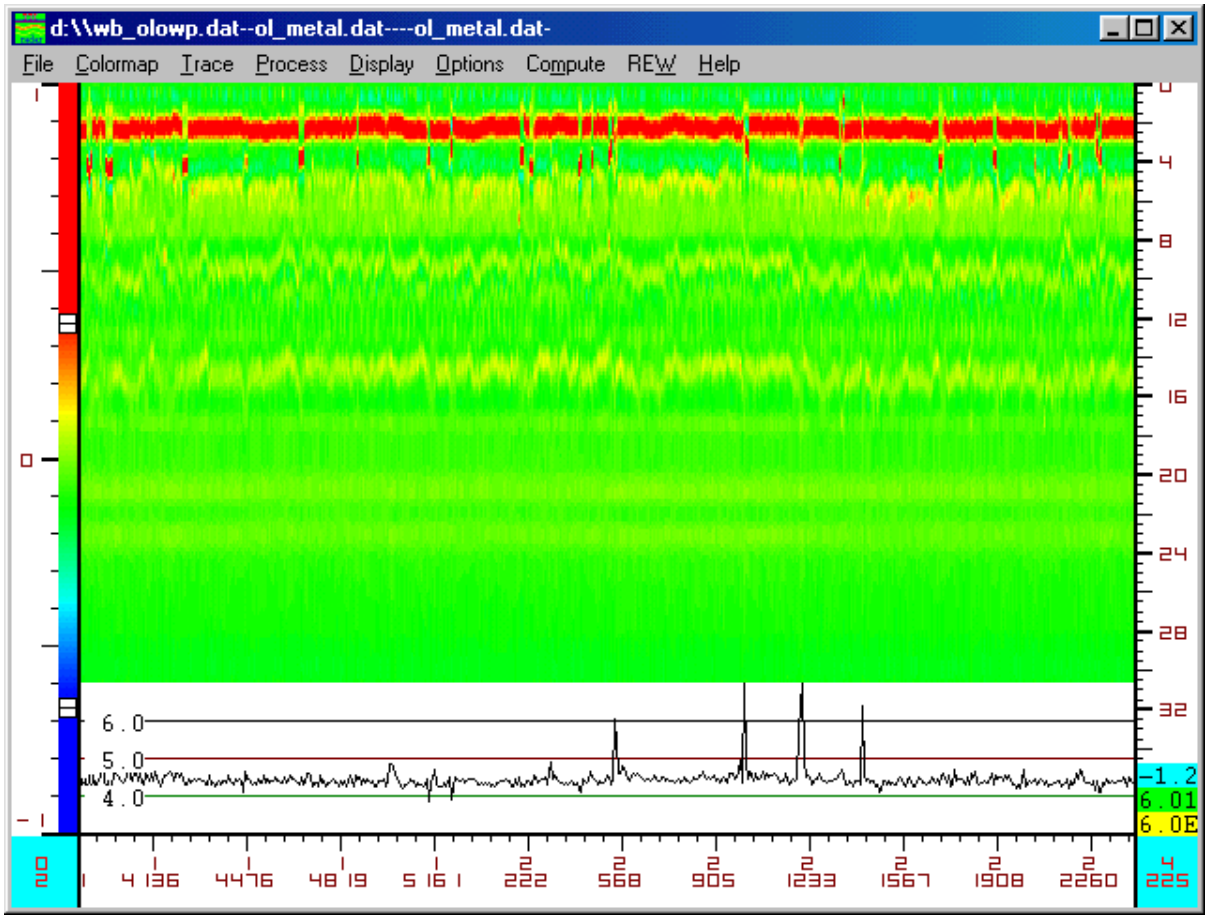

Figure B15. GPR Data Collected along Westbound Outside Lane of I-20 Project (3/4).

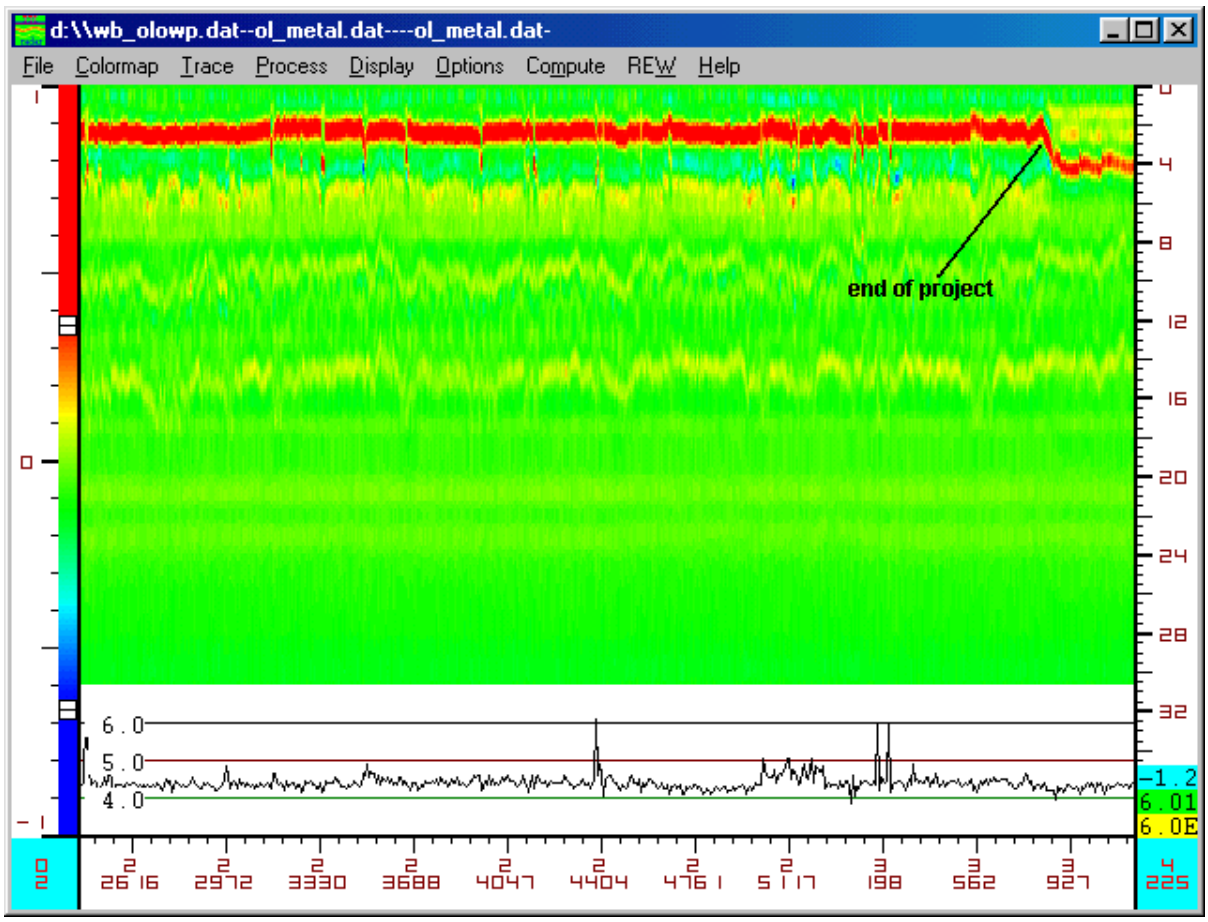

Figure B16. GPR Data Collected along Westbound Outside Lane of I-20 Project (4/4).